

Binary, Gray-Scale, and Vector Soft Mathematical Morphology: Extensions, Algorithms, and Implementations

M. I. VARDAVOULIA, A. GASTERATOS, AND I. ANDREADIS

*Department of Electrical and Computer Engineering,
Democritus University of Thrace, Xanthi, Greece*

| | |
|--|----|
| I. Introduction | 1 |
| II. Standard Mathematical Morphology | 3 |
| A. Binary Morphology | 3 |
| B. Basic Algebraic Properties | 5 |
| C. Gray-scale Morphology with Flat Structuring Elements | 6 |
| D. Gray-scale Morphology with Gray-scale Structuring Elements | 7 |
| E. Vector Morphology for Color Image Processing | 9 |
| F. Fuzzy Morphology | 13 |
| III. Soft Mathematical Morphology | 14 |
| A. Binary Soft Morphology | 14 |
| B. Gray-scale Soft Morphology with Flat Structuring Elements | 15 |
| C. Gray-scale Soft Morphology with Gray-scale Structuring Elements | 16 |
| D. Vector Soft Morphology for Color Image Processing | 16 |
| IV. Soft Morphological Structuring Element Decomposition | 23 |
| V. Fuzzy Soft Mathematical Morphology | 27 |
| A. Definitions | 27 |
| B. Compatibility with Soft Mathematical Morphology | 34 |
| C. Algebraic Properties of Fuzzy Soft Mathematical Morphology | 35 |
| VI. Implementations | 37 |
| A. Threshold Decomposition | 38 |
| B. Majority Gate | 39 |
| 1. Algorithm Description | 39 |
| 2. Systolic Array Implementation for Soft Morphological Filtering | 40 |
| 3. Architecture for Decomposition of Soft Morphological Structuring Elements | 44 |
| C. Histogram Technique | 47 |
| D. Vector Standard Morphological Operation Implementation | 50 |
| VII. Conclusions | 52 |
| References | 52 |

I. INTRODUCTION

Mathematical morphology is an active and growing area of image processing and analysis. It is based on set theory and topology (Matheron, 1975; Serra, 1982; Haralick *et al.*, 1986; Giardina and Dougherty, 1988). Mathematical morphology studies the geometric structure inherent within the image. For

this reason it uses a predetermined geometric shape known as the structuring element. Erosion, which is the basic morphological operation, quantifies the way in which the structuring element fits into the image. Mathematical morphology has provided solutions to many tasks, where image processing can be applied, such as in remote sensing, optical character recognition, radar image sequence recognition, medical imaging, etc. Soft mathematical morphology was introduced by Koskinen *et al.* (1991). In this approach the definitions of the standard morphological operations were slightly relaxed in such a way that a degree of robustness was achieved while most of their desirable properties were maintained. Soft morphological filters are less sensitive to additive noise and to small variations in object shape than standard morphological filters. They have found applications mainly in noise removal, in areas such as medical imaging and digital TV (Harvey, 1998).

The extension of concepts of mathematical morphology to color image processing is not straightforward, because there is not an obvious and unambiguous method of fully ordering vectors (Barnett, 1976). Componentwise morphological techniques, which are based on marginal subordering, do not take into consideration the correlation among color components; thus, they are not vector preserving. Transformation techniques have been used to decorrelate color components and then apply componentwise gray-scale techniques (Goutsias *et al.*, 1995). Morphological techniques that are based on reduced or partial subordering imply the existence of multiple suprema (infima); Thus, they could introduce ambiguity in the resultant data (Comer and Delp, 1998). The crucial point in developing a vector morphology theory for color image processing is the definition of vector-preserving infimum and supremum operators with unique outcome in a properly selected color space.

Another relatively new approach to mathematical morphology is fuzzy mathematical morphology. A fuzzy morphological framework was introduced by Sinha and Dougherty (1992). In this framework the images are treated not as crisp binary sets but as fuzzy sets. Set union and intersection have been replaced by fuzzy bold union and bold intersection, respectively, in order to formulate fuzzy erosion and dilation, respectively. This attempt to adapt mathematical morphology into fuzzy set theory is not unique. Several other attempts have been developed independently by researchers, and they are all described and discussed by Bloch and Maitre (1995). Several fuzzy mathematical morphologies are grouped and compared, and their properties are studied. A general framework unifying all these approaches is also demonstrated.

In this paper recent trends in soft mathematical morphology are presented. The rest of the paper is organized as follows. Binary, gray-scale, and vector standard morphological operations, their algebraic properties, and fuzzy

morphology are discussed in Section II. Soft mathematical morphology is described in Section III. The definitions of vector soft morphological operations, their basic properties, and their use in color impulse noise attenuation are also presented in this section. A soft morphological structuring element-decomposition technique is introduced in Section IV. The definitions of fuzzy soft morphological operations and their algebraic properties are provided in Section V. Several implementations of soft morphological filters and an implementation of vector morphological filters are analyzed in Section VI. Concluding remarks are made in Section VII.

II. STANDARD MATHEMATICAL MORPHOLOGY

The considerations for the structuring element used by Haralick *et al.* (1987) have been adopted for the basic morphological operations. Also, the notations of the extensions of the basic morphological operations (soft morphology, fuzzy morphology and fuzzy soft morphology) are based on the same consideration. Moreover, throughout the paper the discrete case is considered, i.e., all sets belong to the Cartesian grid Z^2 .

A. Binary Morphology

Let the set A denote the image under process and the set B denote the structuring element. Binary erosion and dilation are defined:

$$A \ominus B = \bigcap_{x \in B} (A)_{-x} \quad \text{and} \quad (1)$$

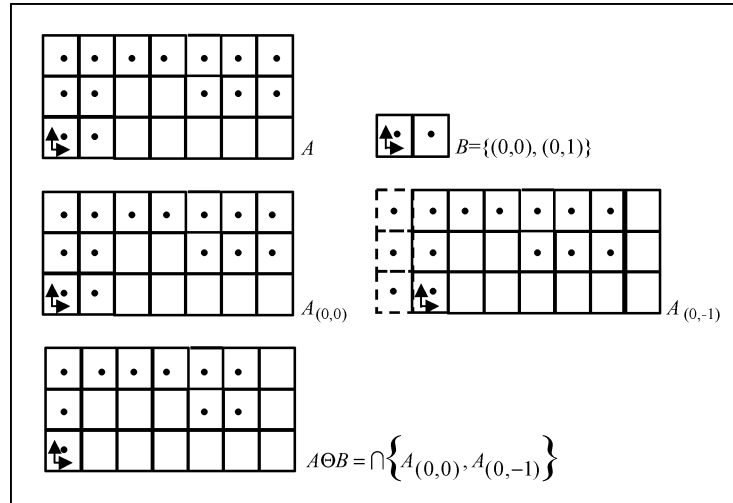
$$A \oplus B = \bigcup_{x \in B} (A)_x, \quad (2)$$

respectively, where A, B are sets of Z^2 and $(A)_x$ is the translation of A by x , which is defined as follows:

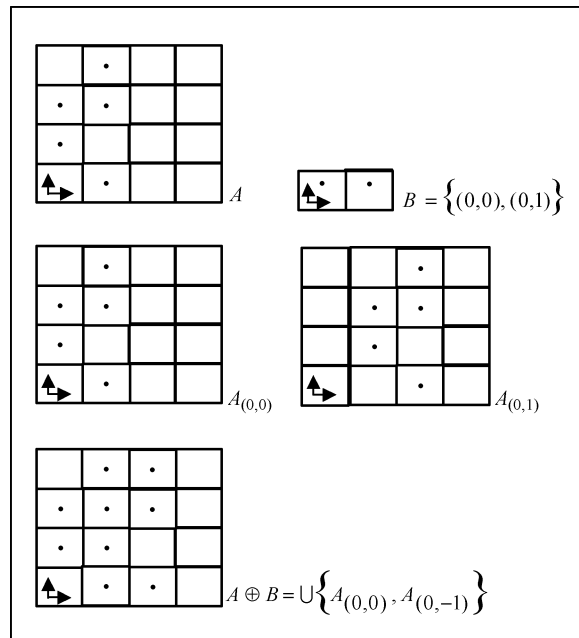
$$(A)_x = \{c \in Z^2 \mid c = a + x \text{ for some } a \in A\} \quad (3)$$

A case of binary erosion and dilation is illustrated in Examples II.1 and II.2, respectively.

Example II.1 $A \ominus B$ results from $A_{(0,0)} \cap A_{(0,-1)}$, according to Eq. (1). The adopted coordinate system is (row, column). The arrows denote the origin of the coordinate system and its direction.



Example II.2 $A \oplus B$ results from $A_{(0,0)} \cup A_{(0,1)}$, according to Eq. (2).



The definitions of binary opening and closing are

$$A \circ B = (A \ominus B) \oplus B \quad \text{and} \quad (4)$$

$$A \bullet B = (A \oplus B) \ominus B, \quad (5)$$

respectively.

B. Basic Algebraic Properties

The basic algebraic properties of the morphological operations are provided in this section.

Theorem II.1 Duality Theorem

Erosion and dilation are dual operations:

$$(A \ominus B)^C = A^C \oplus B^S, \quad (6)$$

where A^C is the complement of A , defined as

$$A^C = \{x \in Z^2 \mid x \notin A\}, \quad (7)$$

and B^S is the reflection of B , defined as

$$B^S = \{x \mid \text{for some } b \in B, x = -b\}. \quad (8)$$

Opening and closing are also dual operations:

$$(A \bullet B)^C = A^C \circ B^S \quad (9)$$

Theorem II.2 Translation Invariance

Both erosion and dilation are translation invariant operations:

$$(A)_x \oplus B = (A \oplus B)_x \quad \text{and} \quad (10)$$

$$(A)_x \ominus B = (A \ominus B)_x, \quad (11)$$

respectively.

Theorem II.3 Increasing Operations

Both erosion and dilation are increasing operations:

$$A \subseteq B \Rightarrow A \ominus C \subseteq B \ominus C, \quad (12)$$

$$A \subseteq B \Rightarrow A \oplus D \subseteq B \oplus D. \quad (13)$$

Theorem II.4 Distributivity

Erosion distributes over set intersection and dilation distributes over set union:

$$(A \cap B) \ominus C = (A \ominus C) \cap (B \ominus C) \quad \text{and} \quad (14)$$

$$(A \cup B) \oplus C = (A \oplus C) \cup (B \oplus C), \quad (15)$$

respectively.

Theorem II.5 *Antiextensivity-Extensivity*

Erosion is an antiextensive operation, provided that the origin belongs to the structuring element:

$$0 \in B \Rightarrow A \ominus B \subseteq A. \quad (16)$$

Similarly, dilation is extensive if the origin belongs to the structuring element:

$$0 \in B \Rightarrow A \subseteq A \oplus B. \quad (17)$$

Theorem II.6 *Idempotency*

Opening and closing are idempotent, i.e., their successive applications do not further change the previously transformed result:

$$A \circ B = (A \circ B) \circ B \quad \text{and} \quad (18)$$

$$A \bullet B = (A \bullet B) \bullet B \quad (19)$$

C. Gray-scale Morphology with Flat Structuring Elements

The definitions of morphological erosion and dilation of a function $f: F \rightarrow Z$ by a flat structuring element (set) B are

$$(f \ominus B)(x) = \min\{f(y) \mid y \in (B)_x\} \quad \text{and} \quad (20)$$

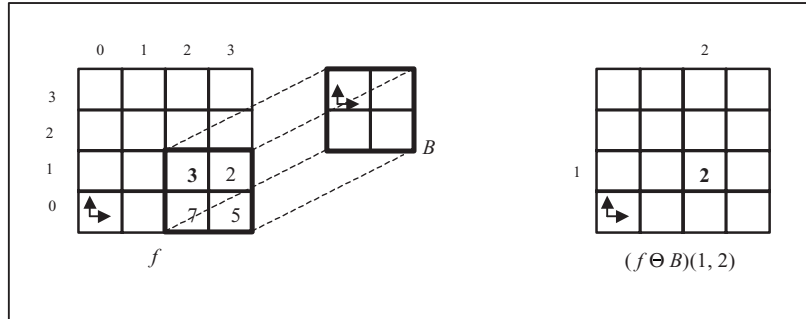
$$(f \oplus B)(x) = \max\{f(y) \mid y \in (B^S)_x\}, \quad (21)$$

respectively, where $x, y \in Z^2$ are the spatial coordinates and $F \subseteq Z^2$ is the domain of the gray-scale image (function).

Examples II.3 and II.4 demonstrate how we can use Eqs. (20) and (21) to perform erosion and dilation, respectively, of a function by a flat structuring element.

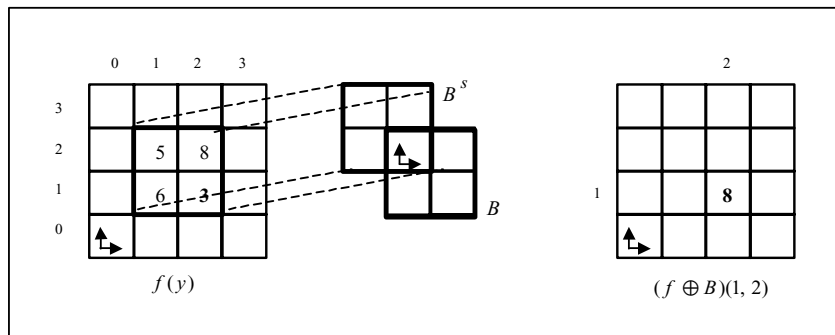
Example II.3 $f(1, 2) = 3$, $x = (1, 2)$, $B = \{(0, 0), (0, 1), (-1, 0), (-1, 1)\}$. According to Eq. (20):

$$\begin{aligned} f \ominus g(1, 2) &= \min\{f(0+1, 0+2), f(0+1, 1+2), f(-1+1, 0+2), \\ &\quad f(-1+1, 1+2)\} \\ &= \min\{f(1, 2), f(1, 3), f(0, 2), f(0, 3)\} = \min\{3, 2, 7, 5\} = 2 \end{aligned}$$



Example II.4 $f(1, 2) = 3$, $x = (1, 2)$, $B = \{(0, 0), (0, 1), (-1, 0), (-1, 1)\}$ and, consequently, $B^S = \{(0, 0), (0, -1), (1, 0), (1, -1)\}$. According to Eq. (21):

$$\begin{aligned} (f \oplus B)(1, 2) &= \max\{f(0 + 1, 0 + 2), f(0 + 1, -1 + 2), f(1 + 1, 0 + 2), \\ &\quad f(1 + 1, -1 + 2)\} \\ &= \max\{f(1, 2), f(1, 1), f(2, 2), f(2, 1)\} \\ &= \max\{3, 6, 8, 5\} = 8. \end{aligned}$$



D. Gray-scale Morphology with Gray-scale Structuring Elements

The definitions of erosion and dilation of a function $f: F \rightarrow Z$ by a gray-scale structuring element $g: G \rightarrow Z$ are

$$(f \ominus g)(x) = \min_{y \in G} \{f(x + y) - g(y)\} \quad \text{and} \quad (22)$$

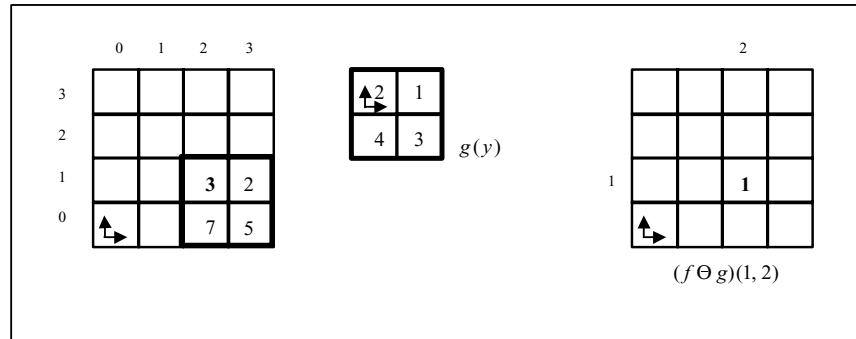
$$(f \oplus g)(x) = \max_{\substack{y \in G \\ x-y \in F}} \{f(x - y) + g(y)\}, \quad (23)$$

respectively, where $x, y \in Z^2$ are the spatial coordinates and $F, G \subseteq Z^2$ are the domains of the gray-scale image (function) and gray-scale structuring element, respectively.

An application of Eqs. (22) and (23) is illustrated in Examples 5 and 6, respectively.

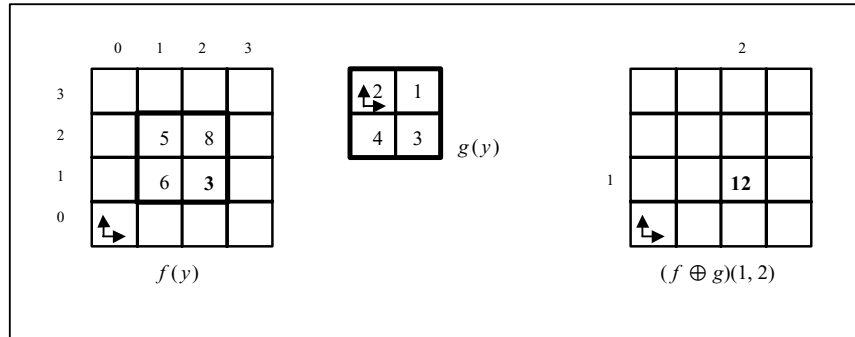
Example II.5 $f(1, 2) = 3, x = (1, 2), G = \{(0, 0), (0, 1), (-1, 0), (-1, 1)\}$. According to Eq. (22):

$$\begin{aligned} f \ominus g(1, 2) &= \min\{f(1+0, 2+0) - g(0, 0), f(1+0, 2+1) - g(0, 1), \\ &\quad f(1-1, 2+0) - g(-1, 0), f(1-1, 2+1) - g(-1, 1)\} \\ &= \min\{f(1, 2) - g(0, 0), f(1, 3) - g(0, 1), f(0, 2) - g(-1, 0), \\ &\quad f(0, 3) - g(-1, 1)\} \\ &= \min\{3 - 2, 2 - 1, 7 - 4, 5 - 3\} \\ &= \min\{1, 1, 3, 2\} = 1. \end{aligned}$$



Example II.6 $f(1, 2) = 3, x = (1, 2), G = \{(0, 0), (0, 1), (-1, 0), (-1, 1)\}$. According to Eq. (23):

$$\begin{aligned} (f \oplus g)(1, 2) &= \max\{f(1-0, 2-0) + g(0, 0), f(1-0, 2-1) + g(0, 1), \\ &\quad f(1+1, 2-0) + g(-1, 0), f(1+1, 2-1) + g(-1, 1)\} \\ &= \max\{f(1, 2) + g(0, 0), f(1, 1) + g(0, 1), f(2, 2) + g(-1, 0), \\ &\quad f(2, 1) + g(-1, 1)\} \\ &= \max\{3 + 2, 6 + 1, 8 + 4, 5 + 3\} \\ &= \max\{5, 7, 12, 8\} = 12 \end{aligned}$$



Gray-scale erosion and dilation possess the properties of binary erosion and dilation, respectively.

E. Vector Morphology for Color Image Processing

Morphological operations suitable for color image processing are defined taking into consideration the following: (1) They should treat colors as vectors (i.e., they should not be componentwise operations), so they can utilize the correlation between color components (Goutsias *et al.*, 1995). (2) They should be vector preserving, so that they do not introduce new vectors (colors) not present in the original data (Talbot *et al.*, 1998). (3) They should produce unique results in all cases, so that they do not introduce ambiguity in the resultant data (Comer and Delp, 1998). (4) They should have the same basic properties with their gray-scale counterparts. (5) They should reduce to their gray-scale counterparts when the vector dimension is 1.

Thus, the definitions for vector morphological operations are extracted by means of vector-preserving supremum and infimum operators, properly defined in a selected color space—i.e., the HSV color space that is user oriented; it depicts colors in a way that approaches human perception. In this space a color is a vector with the components hue ($h \in [0, 360]$), saturation ($s \in [0, 1]$), and value ($v \in [0, 1]$). In the following sections such a color will be denoted by $c(h, s, v)$.

Consider that the HSV space is equipped with the \prec_c conditional suborder relationship (Barnett, 1976), so that

$$c_1(h_1, s_1, v_1) \prec_c c_2(h_2, s_2, v_2) \Leftrightarrow \begin{cases} v_1 < v_2 \\ \text{or} \\ v_1 = v_2 & \text{and } s_1 > s_2 \\ \text{or} \\ v_1 = v_2 & \text{and } s_1 = s_2 & \text{and } h_1 < h_2 \end{cases} \quad (24)$$

10 M. I. VARDAVOULIA, A. GASTERATOS, AND I. ANDREADIS

and

$$c_1(h_1, s_1, v_1) \underset{c}{=} c_2(h_2, s_2, v_2) \Leftrightarrow v_1 = v_2 \quad \text{and} \quad s_1 = s_2 \quad \text{and} \quad h_1 = h_2 \quad (25)$$

Then, if SB_n is an arbitrary subset of the HSV space, which includes n vectors $c_1(h_1, s_1, v_1), c_2(h_2, s_2, v_2), \dots, c_n(h_n, s_n, v_n)$, the $\underset{c}{\wedge}$ infimum operator in SB_n is defined as follows:

$$\begin{aligned} \underset{c}{\wedge} SB_n &= \underset{c}{\wedge} \{c_1(h_1, s_1, v_1), c_2(h_2, s_2, v_2), \dots, c_n(h_n, s_n, v_n)\} \\ &= c_k(h_k, s_k, v_k) : \begin{cases} v_k = \min\{v_1, v_2, \dots, v_n\} \\ \text{if } \nexists i \neq j : v_i = v_j = \min\{v_1, v_2, \dots, v_n\} \\ \quad 1 \leq i, j \leq n \\ \text{or} \\ v_k = v_i = v_j = \min\{v_1, v_2, \dots, v_n\} \text{ and} \\ s_k = \max\{s_i, s_j\} \\ \text{if } \exists i \neq j : v_i = v_j = \min\{v_1, v_2, \dots, v_n\} \text{ and } s_i \neq s_j \\ \quad 1 \leq i, j \leq n \\ \text{or} \\ v_k = v_i = v_j = \min\{v_1, v_2, \dots, v_n\} \text{ and} \\ s_k = \max\{s_i, s_j\} \text{ and } h_k = \min\{h_i, h_j\} \\ \text{if } \exists i \neq j : v_i = v_j = \min\{v_1, v_2, \dots, v_n\} \text{ and } s_i = s_j \\ \quad 1 \leq i, j \leq n \end{cases} \end{aligned} \quad (26)$$

The $\underset{c}{\vee}$ supremum operator in SB_n is defined in a similar way.

From previous definition it is obvious that the $\underset{c}{\wedge}$ and $\underset{c}{\vee}$ operators are vector preserving, because they always produce as a result one of the input vectors included in SB_n . These operators are used to define vector morphological operations that are vector preserving, as well.

Let us consider two functions $f, g : R^n \rightarrow \text{HSV}$, i.e., two n -dimensional color images, where f is the image under process (the input image) and g is the structuring element. If $f(x) = c(h_{xf}, s_{xf}, v_{xf})$, $x \in R^n$, then the definitions of vector erosion and dilation, respectively, are

$$(f \ominus g)(x) = \underset{c}{\wedge} \{f(x+y) - g(y)\} \quad (27)$$

$$(f \oplus g)(x) = \underset{c}{\vee} \{f(x-y) + g(y)\} \quad (28)$$

where $x, y \in R^n$ are the spatial coordinates and $F, G \subseteq R^n$ are the domains of the color input image (function) and the color structuring element, respectively. Moreover, \ominus, \oplus denote vector subtraction and addition, respectively, which are defined as follows:

$$f(k) - g(k) = c(h_{kf} - h_{kg}, s_{kf} - s_{kg}, v_{kf} - v_{kg}), \quad k \in R^n \quad (29)$$

with

$$\begin{aligned} h_{kf} - h_{kg} &= 0 && \text{if } h_{kf} - h_{kg} < 0 \\ s_{kf} - s_{kg} &= 0 && \text{if } s_{kf} - s_{kg} < 0 \\ v_{kf} - v_{kg} &= 0 && \text{if } v_{kf} - v_{kg} < 0 \end{aligned}$$

and

$$f(k) + g(k) = c(h_{kf} + h_{kg}, s_{kf} + s_{kg}, v_{kf} + v_{kg}) \quad (30)$$

with

$$\begin{aligned} h_{kf} + h_{kg} &= 360 && \text{if } h_{kf} + h_{kg} > 360 \\ s_{kf} + s_{kg} &= 1 && \text{if } s_{kf} + s_{kg} > 1 \\ v_{kf} - v_{kg} &= 1 && \text{if } v_{kf} + v_{kg} > 1 \end{aligned}$$

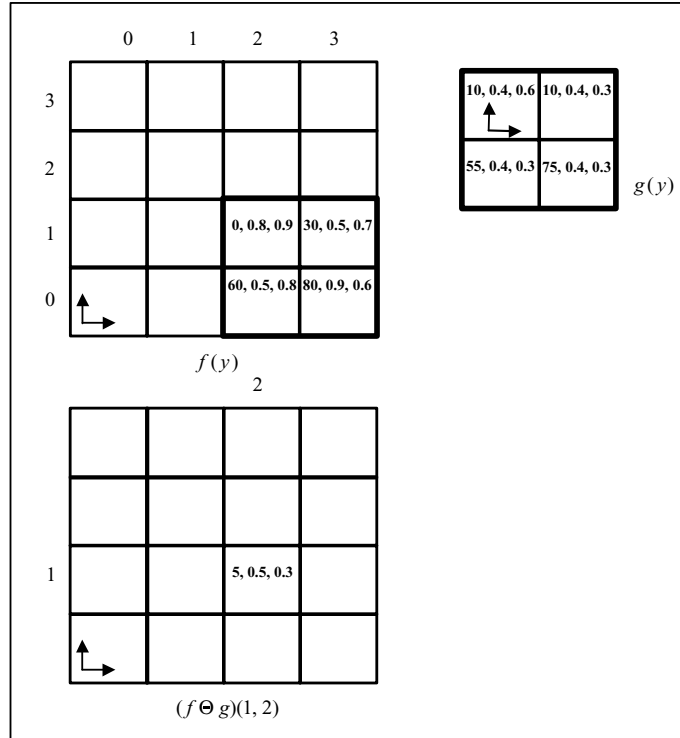
Vector opening and closing are defined similarly to their gray-scale counterparts.

It has been proven that the defined vector morphological operations possess the same basic properties with their gray-scale counterparts: extensivity or antiextensivity, increasing or decreasing monotony, translation invariance, and duality. In addition, they are identical to their gray-scale counterparts when the vector dimension is 1. Consequently, the proposed vector morphology is compatible to gray-scale morphology.

Examples II.7 and II.8 demonstrate the cases of vector erosion and dilation, respectively.

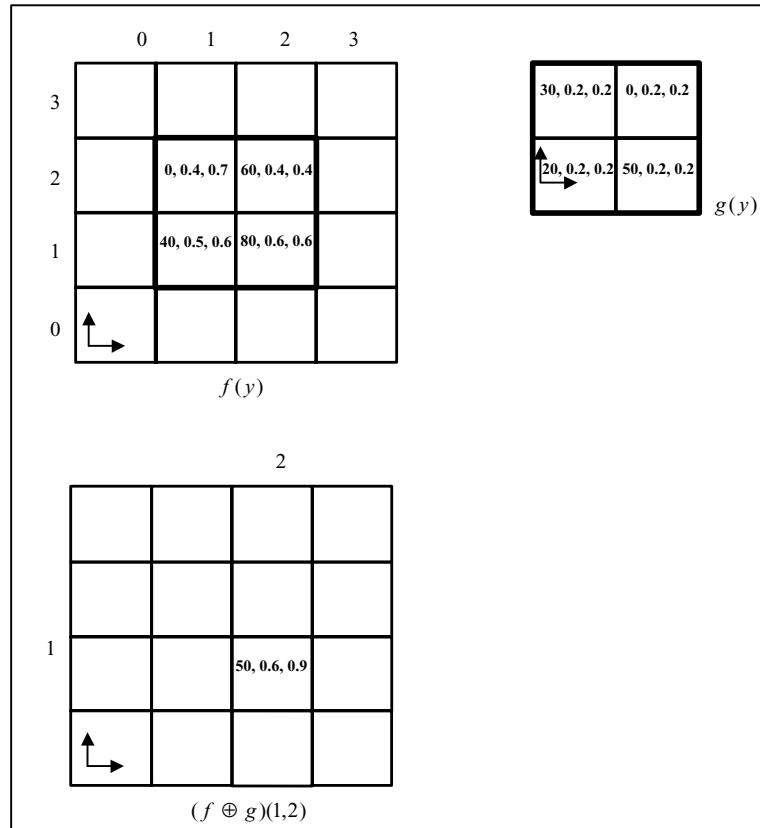
Example II.7 $f(1, 2) = c(0, 0.8, 0.9)$, $x = (1, 2)$, $G = \{(0, 0), (0, 1), (-1, 0), (-1, 1)\}$. According to Eq. (27):

$$\begin{aligned} f \ominus g(1, 2) &= \wedge_c \{f(1+0, 2+0) - g(0, 0), f(1+0, 2+1) - g(0, 1), \\ &\quad f(1-1, 2+0) - g(-1, 0), f(1-1, 2+1) - g(-1, 1)\} \\ &= \wedge_c \{f(1, 2) - g(0, 0), f(1, 3) - g(0, 1), f(0, 2) - g(-1, 0), \\ &\quad f(0, 3) - g(-1, 1)\} \\ &= \wedge_c \{c(0, 0.8, 0.9) - c(10, 0.4, 0.6), c(30, 0.5, 0.7) \\ &\quad - c(10, 0.4, 0.3), c(60, 0.5, 0.8) \\ &\quad - c(55, 0.4, 0.3), c(80, 0.9, 0.6) - c(75, 0.4, 0.3)\} \\ &= \wedge_c \{c(0, 0.4, 0.3), c(20, 0.1, 0.4), c(5, 0.1, 0.5), c(5, 0.5, 0.3)\} \\ &= c(5, 0.5, 0.3) \end{aligned}$$



Example II.8 $f(1, 2) = c(80, 0.6, 0.6)$, $x = (1, 2)$, $G = \{(0, 0), (0, 1), (-1, 0), (-1, 1)\}$. According to Eq. (28):

$$\begin{aligned}
 (f \oplus g)(1, 2) &= \vee_c \{f(1 - 0, 2 - 0) + g(0, 0), f(1 - 0, 2 - 1) + g(0, 1), \\
 &\quad f(1 + 1, 2 - 0) + g(-1, 0), f(1 + 1, 2 - 1) + g(-1, 1)\} \\
 &= \vee_c \{f(1, 2) + g(0, 0), f(1, 1) + g(0, 1), f(2, 2) + g(-1, 0), \\
 &\quad f(2, 1) + g(-1, 1)\} \\
 &= \vee_c \{c(80, 0.6, 0.6) + c(30, 0.2, 0.2), c(40, 0.5, 0.6) \\
 &\quad + c(0, 0.2, 0.2), c(60, 0.4, 0.4) \\
 &\quad + c(20, 0.2, 0.2), c(0, 0.4, 0.7) + c(50, 0.2, 0.2)\} \\
 &= \vee_c \{c(110, 0.8, 0.8), c(40, 0.7, 0.8), c(80, 0.6, 0.6), \\
 &\quad c(50, 0.6, 0.9)\} = c(50, 0.6, 0.9)
 \end{aligned}$$



F. Fuzzy Morphology

In this paper the definitions introduced by Sinha and Dougherty (1992) are used. These are a special case of the framework presented by Bloch and Maitre (1995). In this approach, fuzzy mathematical morphology is studied in terms of fuzzy fitting. The fuzziness is introduced by the degree to which the structuring element fits into the image. The operations of erosion and dilation of a fuzzy image by a fuzzy structuring element having a bounded support are defined in terms of their membership functions:

$$\begin{aligned} \mu_{A \ominus B}(x) &= \min_{y \in B} [\min[1, 1 + \mu_A(x + y) - \mu_B(y)]] \\ &= \min_{y \in B} [1, \min[1, +\mu_A(x + y) - \mu_B(y)]] \end{aligned} \quad (31)$$

14 M. I. VARDAVOULIA, A. GASTERATOS, AND I. ANDREADIS

and

$$\begin{aligned}\mu_{A\oplus B}(x) &= \max_{y \in B} [\max[0, \mu_A(x - y) + \mu_B(y) - 1]] \\ &= \max_{y \in B} [0, \mu_A(x - y) + \mu_B(y) - 1]\end{aligned}\quad (32)$$

where $x, y \in Z^2$ are the spatial coordinates and μ_A, μ_B are the membership functions of the image and the structuring element, respectively.

It is obvious from Eqs. (31) and (32) that the results of both fuzzy erosion and dilation have membership functions whose values are within the interval $[0, 1]$.

III. SOFT MATHEMATICAL MORPHOLOGY

In soft morphological operations, the maximum or the minimum operations used in standard gray-scale morphology are replaced by weighted order statistics. A weighted order statistic is a certain element of a list, the members of which have been ordered. Some of the members from the original unsorted list, participate with a weight greater than 1, i.e. they are repeated more than once, before sorting (David, 1981; Pitas and Venetsanopoulos, 1990). Furthermore, in soft mathematical morphology the structuring element B is divided into two subsets; the core B_1 and the soft boundary B_2 .

A. Binary Soft Morphology

The basic definitions of the binary soft erosion and dilation are (Pu and Shih, 1995):

$$(A \ominus [B_1, B_2, k])(x) = \{x \in A \mid (k \times \text{Card}[A \cap (B_1)_x] + \text{Card}[A \cap (B_2)_x]) \geq k \text{Card}[B_1] + \text{Card}[B_2] - k + 1\} \quad (33)$$

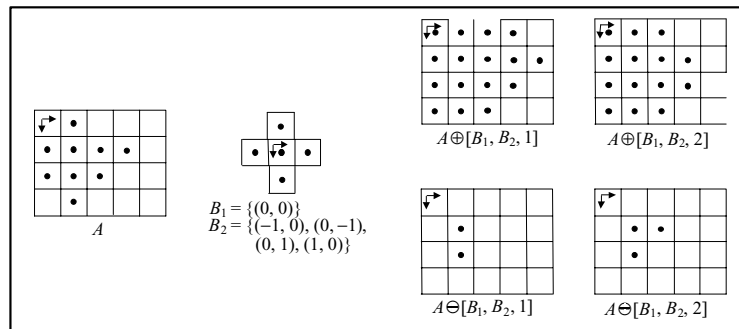
and

$$(A \oplus [B_1, B_2, k])(x) = \{x \in A \mid (k \times \text{Card}[A \cap (B_1^S)_x] + \text{Card}[A \cap (B_2^S)_x]) \geq k\} \quad (34)$$

respectively, where k is called the order index, which determines the number of times that the elements of core participate into the result, and $\text{Card}[X]$ denotes the cardinality of set X , i.e., the number of the elements of X .

In the extreme case when the order index $k=1$ or, alternatively, $B = B_1 (B_2 = \emptyset)$, soft morphological operations are reduced to standard morphological operations.

Example III.1 The following example demonstrates a case of soft binary dilation and erosion.



If $k > \text{Card}[B_2]$, soft morphological operations are affected only by the core B_1 , i.e., using B_1 as the structuring element. Therefore, in this case the nature of soft morphological operations is not preserved (Kuosmanen and Astola, 1995; Pu and Shih, 1995). For this reason the constraint $k \leq \min\{\text{Card}(B)/2, \text{Card}(B_2)\}$ is used. In the preceding example $\min(\text{Card}(B)/2, \text{Card}(B_2)) = 2.5$; therefore, only the cases $k=1$ and $k=2$ are considered. For $k=1$ the results of both dilation and erosion are the same as those that would have been obtained by applying Eqs. (2) and (1), respectively.

B. Gray-scale Soft Morphology with Flat Structuring Elements

The definitions of soft morphology were first introduced by Koskinen *et al.* (1991) as transforms of a function by a set. In the definition of soft dilation, the reflection of the structuring element is used, so that in the case of $k=1$ the definitions comply with (Haralick *et al.*, 1986).

$$(f \ominus [B_1, B_2, k])(x) = \min^{(k)}(\{k \diamond f(y) \mid y \in (B_1)_x\} \cup \{f(z) \mid z \in (B_2)_x\}) \quad (35)$$

and

$$(f \oplus [B_1, B_2, k])(x) = \max^{(k)}(\{k \diamond (y) \mid y \in (B_1^S)_x\} \cup \{f(z) \mid z \in (B_2^S)_x\}) \quad (36)$$

respectively, where $\min^{(k)}$ and $\max^{(k)}$ are the k th smallest and the k th largest element of the multiset, respectively; a multiset is a collection of objects, where the repetition of objects is allowed and the symbol \diamond denotes the repetition, i.e., $\{k \diamond f(x)\} = \{f(x), f(x), \dots, f(x)\}$ (k times).

C. Gray-scale Soft Morphology with Gray-scale Structuring Elements

Soft morphological erosion of a gray-scale image $f: F \rightarrow Z$ by a soft gray-scale structuring element $[\alpha, \beta, k]: B \rightarrow Z$ is (Pu and Shih, 1995):

$$f \ominus [\alpha, \beta, k](x) = \min_{\substack{y \in B_1 \\ z \in B_2}}^{(k)} (\{k \diamond (f(x+y) - \alpha(y))\} \cup \{f(x+z) - \beta(z)\}) \quad (37)$$

Soft morphological dilation of f by $[\alpha, \beta, k]$ is

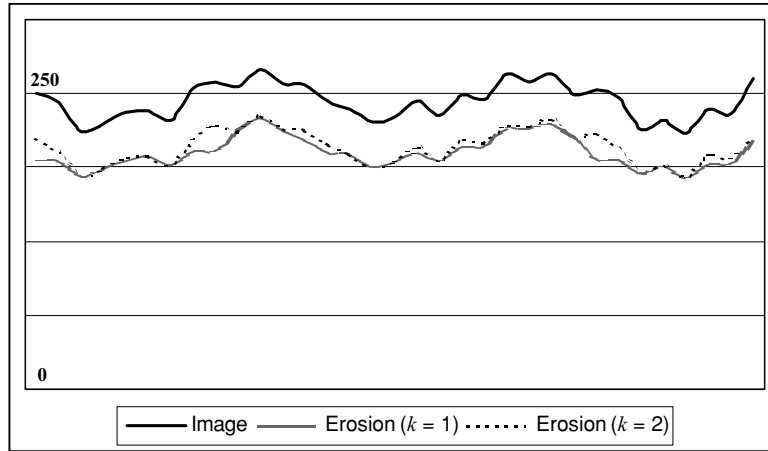
$$f \oplus [\alpha, \beta, k](x) = \max_{\substack{(x-y), (x-z) \in F \\ z \in B_1 \\ z \in B_2}}^{(k)} (\{k \diamond (f(x-y) + \alpha(y))\} \cup \{f(x-z) - \beta(z)\}) \quad (38)$$

where $x, y, z \in Z^2$ are the spatial coordinates, $\alpha: B_1 \rightarrow Z$ is the core of the gray-scale structuring element, $\beta: B_2 \rightarrow Z$ is the soft boundary of the gray-scale structuring element, and $F, B_1, B_2 \subseteq Z^2$ are the domains of the gray-scale image, the core of the gray-scale structuring element, and the soft boundary of the gray-scale structuring element, respectively.

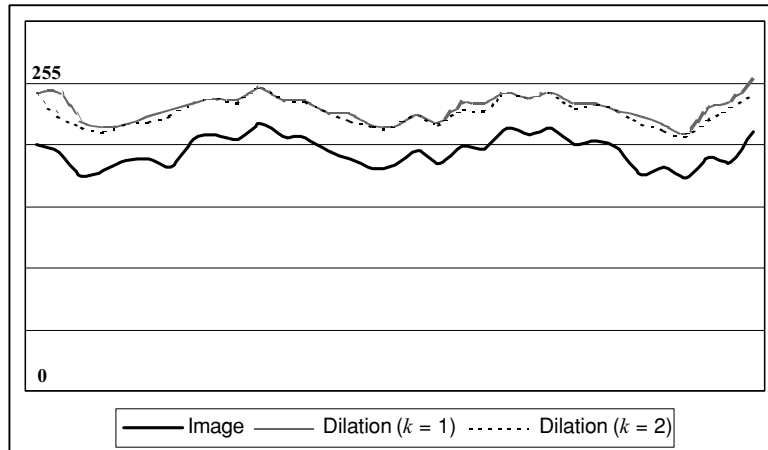
Figure 1 demonstrates one-dimensional soft morphological operations and the effect of the order index k . The same structuring element is used for both operations. It is a one-dimensional structuring element with five discrete values. The central value corresponds to its core and it is equal to 30. Additionally, it denotes the origin. The four remaining values belong to its soft boundary and they are equal to 20. From both Figures 1a and b it is obvious that the greater the value of the order index, the better the fitting.

D. Vector Soft Morphology for Color Image Processing

In this section an approach to soft color image mathematical morphology is presented. This extends the vector standard morphology theory discussed in Section II.E in the same way that gray-scale soft morphology extends the gray-scale standard morphology theory. Vector soft morphology, like gray-scale soft morphology, aims at improving the behavior of vector standard morphological



(a)



(b)

FIGURE 1. Illustration of one-dimensional soft morphological operations and the effect of the order index k ; (a) soft erosion and (b) soft dilation.

filters in noisy environments. It retains the concept of splitting the structuring element in two parts: the core and the soft boundary. It also preserves the concept of the order index k , which implies that the core “weights” more than the soft boundary in the calculation of the result. Furthermore, it uses the relational operator $<$ (Eq. (24)) in order to rank the vector values included in

a multiset of HSV space vectors. Here again the k th-order statistic is the result of the vector soft morphological operation.

Let SB_n be an arbitrary subset of the HSV space, which includes n vectors c_1, c_2, \dots, c_n , and $SB_{n(\text{ord})}$ be the set of the ordered values $c_{(1)}, c_{(2)}, \dots, c_{(n)}$ i.e.,

$$SB_{n(\text{ord})} = \{c_{(1)}, c_{(2)}, \dots, c_{(n)}\}, c_{(1)} \leq_c c_{(2)} \leq_c \dots \leq_c c_{(n)}.$$

Then the k th smallest and the k th largest vector, respectively, in SB_n are

$$\min_c^{(k)}(SB_n) = c_{(k)}, \quad 1 \leq k \leq n \quad (39)$$

and

$$\max_c^{(k)}(SB_n) = c_{(n-k+1)}, \quad 1 \leq k \leq n \quad (40)$$

Therefore, vector soft erosion and dilation of a color image f by a color structuring element $g(f, g : R^n \rightarrow \text{HSV})$ are defined as follows.

$$(f \ominus [\beta, \alpha, k])(x) = \min_c^{(k)}(\{k \diamond (f(x+y) - a(y))\} \cup \{f(x+z) - \beta(z)\})$$

$$\begin{matrix} y \in B_1 \\ z \in B_2 \end{matrix} \quad (41)$$

$$(f \oplus [\beta, \alpha, k])(x) = \max_c^{(k)}(\{k \diamond (f(x+y) + a(y))\} \cup \{f(x-z) + \beta(z)\})$$

$$\begin{matrix} (x-y), (x-z) \in F \\ z \in B_1 \\ z \in B_2 \end{matrix} \quad (42)$$

where $x, y, z \in R^n$ are the spatial coordinates, $a: B_1 \rightarrow R^n$ is the core of the color structuring element, $\beta: B_2 \rightarrow R^n$ is the soft boundary of the color structuring element, and $F, B_1, B_2 \subseteq R^n$ are the domains of the color image, the core of the color structuring element, and the soft boundary of the color structuring element, respectively. In addition, $(-)$ and $(+)$ are the vector subtraction and addition operations defined in Eqs. (29) and (30), respectively. Vector soft opening and closing are defined similarly to their gray-scale counterparts.

Vector soft morphology is compatible to gray-scale soft morphology. In vector soft morphology, as in gray-scale soft morphology, the restriction $k \leq \min\{\text{Card}(B)/2, \text{Card}(B_2)\}$ for the order index k ensures that the nature of soft morphological operations is preserved. Moreover, primary and secondary operations of vector soft morphology are reduced to their gray-scale counterparts when they are applied to gray-scale images. In addition, vector soft erosion,

dilation opening, and dilation closing possess the same basic properties with gray-scale soft erosion, dilation, opening, and closing, respectively.

Theorem III.1 *Duality Theorem*

Vector soft erosion and dilation are dual operations:

$$-(f \oplus [\beta, \alpha, k])(x) = (-f \ominus [\beta', \alpha', k])(x) \quad (43)$$

Vector soft opening and closing are also dual operations:

$$-(f \circ [\beta, \alpha, k]) = -f \bullet [\beta', \alpha', k] \quad (44)$$

Theorem III.2 *Translation Invariance*

Vector soft erosion and dilation are translation invariant:

$$(f \ominus [\beta, \alpha, k])_y + j = (f_y + j) \ominus [\beta, \alpha, k], \quad y \in R^n, j \in \text{HSV} \quad (45)$$

$$(f \oplus [\beta, \alpha, k])_y + j = (f_y + j) \oplus [\beta, \alpha, k], \quad y \in R^n, j \in \text{HSV} \quad (46)$$

Vector soft opening and closing are translation invariant, as well:

$$(f \circ [\beta, \alpha, k])_y + j = (f_y + j) \circ [\beta, \alpha, k], \quad y \in R^n, j \in \text{HSV} \quad (47)$$

$$(f \bullet [\beta, \alpha, k])_y + j = (f_y + j) \bullet [\beta, \alpha, k], \quad y \in R^n, j \in \text{HSV} \quad (48)$$

Theorem III.3 *Increasing Operations*

Vector soft erosion and dilation are monotonically increasing operations:

$$f_1 \ll f_2 \Rightarrow \begin{cases} f_1 \ominus [\beta, \alpha, k] \ll f_2 \ominus [\beta, \alpha, k] \\ f_1 \oplus [\beta, \alpha, k] \ll f_2 \oplus [\beta, \alpha, k] \end{cases} \quad (49)$$

where $g \ll f \Leftrightarrow G \subseteq F$ and $g(x) \leq_c f(x) \forall x \in G$.

Vector opening and closing are monotonically increasing operations, as well:

$$f_1 \ll f_2 \Rightarrow \begin{cases} f_1 \circ [\beta, \alpha, k] \ll f_2 \circ [\beta, \alpha, k] \\ f_1 \bullet [\beta, \alpha, k] \ll f_2 \bullet [\beta, \alpha, k] \end{cases} \quad (50)$$

Theorem III.4 *Extensivity–antiextensivity*

If the origin lies inside the core of the structuring element, vector soft erosion is antiextensive and vector soft dilation is extensive:

$$0 \in \alpha \Rightarrow \begin{cases} (f \ominus [\beta, \alpha, k])(x) \leq_c f(x) \\ (f \oplus [\beta, \alpha, k])(x) \geq_c f(x) \end{cases} \quad (51)$$

On the contrary, vector soft opening is not in general antiextensive and vector soft closing is not in general extensive:

$$\exists x \in R^n : \begin{cases} (f \circ [\beta, \alpha, k])(x) \underset{c}{\geq} f(x) \\ (f \bullet [\beta, \alpha, k])(x) \underset{c}{\geq} f(x) \end{cases} \quad (52)$$

Theorem III.5 *Idempotency*

Like their gray-scale counterparts, vector soft opening and closing are not, in general, idempotent.

$$\exists f, g : R^n \rightarrow \text{HSV} \text{ such that } \begin{cases} f \circ [\beta, \alpha, k] \neq (f \circ [\beta, \alpha, k]) \circ [\beta, \alpha, k] \\ f \bullet [\beta, \alpha, k] \neq (f \bullet [\beta, \alpha, k]) \bullet [\beta, \alpha, k] \end{cases} \quad (53)$$

The main characteristic of morphological methods is that they take into consideration the geometrical shape of the objects to be analyzed. However, standard morphological operations are highly sensitive to noise. In some applications this sensitivity may cause problems: prefiltering to remove noise is necessary; if this prefiltering is not done very carefully, it may result in corruption of the shape of objects to be studied, thus degrading the overall performance of the system. Gray-scale soft mathematical morphology was introduced by Koskinen *et al.* (1991), as an extension of gray-scale standard mathematical morphology, in order to improve the behavior of gray-scale standard morphological filters in noisy environments: gray-scale soft morphological operations are less sensitive to impulse noise and to small variations in object shape (Koskinen and Astola, 1994) compared to the corresponding gray-scale standard morphological operations. Experimental results show that vector soft morphological operations act in a similar way with their gray-scale counterparts: they are advantageous regarding small detail preservation and impulse noise attenuation in comparison to the corresponding vector standard morphological operations. This is illustrated in Figures 2 and 3.

More specifically, Figure 2 demonstrates the effect of the order index k in object shape and small detail preservation. From Figures 2b–d it is obvious that, as in gray-scale soft morphology, the greater the value of the order index, the better the detail preservation. Comparing Figures 2b–d, it can be also observed that the smaller the value of k , the closer the behavior of a vector soft morphological transform is to that of the corresponding vector standard morphological transform, just as in the case of soft gray-scale morphology (Kuusmanen and Astola, 1995). This is one more similarity of vector soft and gray-scale soft



FIGURE 2. (a) Original color image “Veta,” (b) image after vector standard erosion by $g = [\beta, \alpha, 1]$, (c) image after vector soft erosion by $[\beta, \alpha, 2]$, and (d) image after vector soft erosion by $[\beta, \alpha, 4]$.

morphological transforms. For instance, in Figure 2 it can be seen that, for soft vector erosion, $f \ominus g \leq f \ominus [\beta, \alpha, k] \leq f \ominus [\beta, \alpha, k + 1] \leq f$, which holds for gray-scale soft erosion as well.

Figure 3 illustrates that vector soft morphological transforms are advantageous in color impulse noise elimination, in comparison to the corresponding



(a)



(b)



(c)



(d)



(e)

vector standard morphological transforms. It can be seen that vector soft opening (closing) removes both positive and negative color impulse noise, just as in the gray-scale case. It can also be observed that the increase of the order index k increases the noise-removal capability and the detail-preservation capability, as well.

At this point it must be mentioned that a significant problem in the study of impulse noise removal from color images is the lack of a generally accepted multivariate impulse noise model. Recently various such models have been proposed. The following color impulse noise model (Plataniotis *et al.*, 1999) has been used in our experiments:

$$c_n = \begin{cases} c_0 = c(h, s, v) & \text{with probability } (1 - p) \\ c(d, s, v) & \text{with probability } p_1 p \\ c(h, d, v) & \text{with probability } p_2 p \\ c(h, s, d) & \text{with probability } p_3 p \\ c(d, d, d) & \text{with probability } p_S p \end{cases} \quad (54)$$

where c_0 is the original vector (the noncontaminated color), c_n is the noisy vector, and d is the impulse value. Furthermore, P is the degree of impulse noise distortion, $p_S = 1 - (p_1 + p_2 + p_3)$, and $p_1 + p_2 + p_3 \leq 1$. The positive or negative impulse value d is properly placed in the range of each vector component.

IV. SOFT MORPHOLOGICAL STRUCTURING ELEMENT DECOMPOSITION

A soft morphological structuring element decomposition technique is described in this section (Gasteratos *et al.*, 1998c). According to this technique, the domain B of the structuring element is divided into smaller, nonoverlapping subdomains B_1, B_2, \dots, B_n . Also, $B_1 \cup B_2 \cup \dots \cup B_n = B$. The soft morphological structuring elements obtain values from these domains, and they are denoted by $[\lambda_1, \mu_1, k], [\lambda_2, \mu_2, k], \dots, [\lambda_n, \mu_n, k]$, respectively. These have a common origin, which is the origin of the original structuring element. Additionally, the points of B that belong to its core are also points of the cores of B_1, B_2, \dots, B_n and the points of B that belong to the soft boundary are also points of the soft boundaries of B_1, B_2, \dots, B_n . This process is graphically illustrated

FIGURE 3. (a) Original color image "Veta's birthday," (b) image corrupted by 6% positive and negative HSV impulse noise with $p_1 = p_2 = p_3 = 0$ and $p_S = 1$, (c) resulting image after vector standard opening by $g = [\beta, \alpha, 1]$, (d) resulting image after vector soft opening by $[\beta, \alpha, 2]$, and (e) resulting image after vector soft opening by $[\beta, \alpha, 4]$.

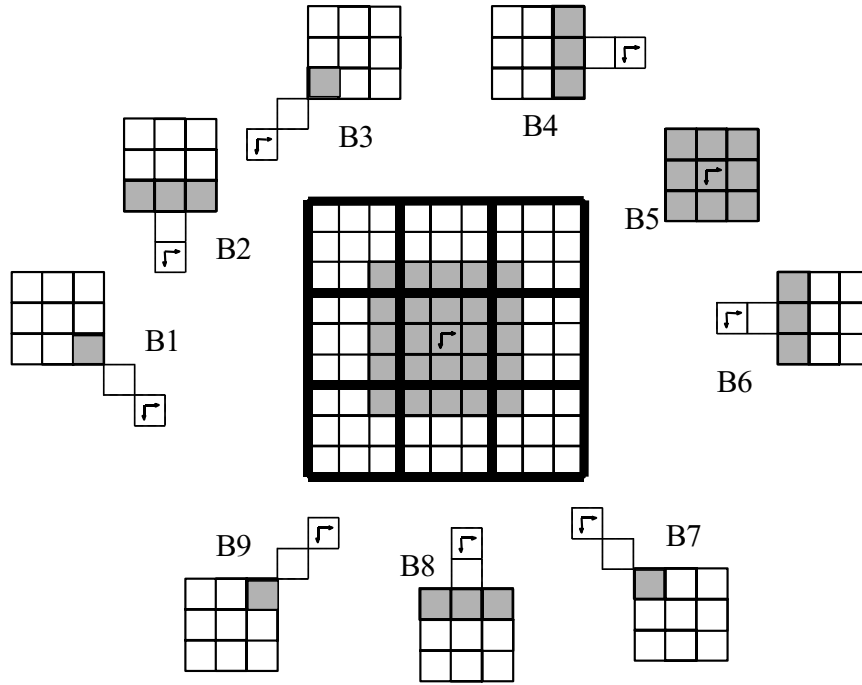


FIGURE 4. Example of a 4×4 soft morphological structuring element decomposition.

in Figure 4. In this figure the core of the structuring element is denoted by the shaded area.

Soft dilation and erosion are computed as follows:

$$f \oplus [\alpha, \beta, k](x) = \max_{i=1}^n \max_{\substack{(x-y) \in B_1 \\ (x-z) \in B_2 \\ j=1}}^{(k)} \{ \{k \diamond (f(x-y) + \lambda_i(y))\} \cup \{f(x-z) + \mu_i(z)\} \} \quad (55)$$

$$f \ominus [\alpha, \beta, k](x) = \max_{i=1}^n \max_{\substack{(x-y) \in B_1 \\ (x-z) \in B_2 \\ j=1}}^{(k)} \{ \{k \diamond (f(x+y) - \lambda_i(y))\} \cup \{f(x+z) - \mu_i(z)\} \} \quad (56)$$

respectively, where B_1 and B_2 are the domain of the core and the soft boundary of the large structuring element $[\alpha, \beta, k]: B \rightarrow Z$.

Proof.

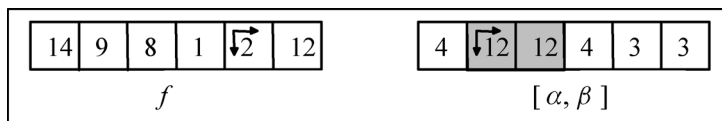
$$\begin{aligned}
\forall y \in B_1 : \alpha(y) &= \bigcup_{i=1}^n \lambda_i(y) \\
\Rightarrow f(x-y) + \alpha(y) &= \bigcup_{i=1}^n [f(x-y) + \lambda_i(y)], \quad (x-y) \in B_1 \\
\Rightarrow k \diamond (f(x-y) + \alpha(y)) &= k \diamond \left(\bigcup_{i=1}^n [f(x-y) + \lambda_i(y)] \right) \\
&= k \diamond (f(x-y) + \lambda_1(y), f(x-y) \\
&\quad + \lambda_2(y), \dots, f(x-y) + \lambda_n(y)), (x-y) \in B_1
\end{aligned} \tag{57}$$

Also,

$$\begin{aligned}
\forall z \in B_2 : \beta(z) &= \bigcup_{i=1}^n \mu_i(z) \\
\Rightarrow f(x-z) + \beta(z) &= \bigcup_{i=1}^n [f(x-z) + \mu_i(z)] \\
&= f(x-z) + \mu_1(z), f(x-z) + \mu_2(z), \dots, \\
&\quad f(x-z) + \mu_n(z), \quad (x-z) \in B_2
\end{aligned} \tag{58}$$

Through Eqs. (38), (57), and (58) we obtain:

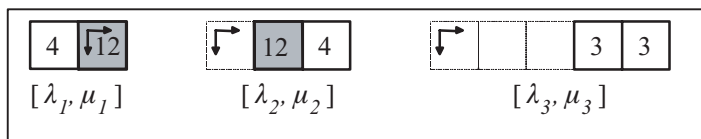
$$\begin{aligned}
&f \oplus [\alpha, \beta, k](x) \\
&= \max_{\substack{(x-y) \in B_1 \\ (x-z) \in B_2}}^{(k)} \left(\begin{array}{l} \{k \diamond (f(x-y) + \lambda_1(y), f(x-y) \\ + \lambda_2(y), \dots, f(x-y) + \lambda_n(y))\} \cup \\ \{f(x-z) + \mu_1(z), f(x-z) + \mu_2(z), \dots, \\ f(x-z) + \mu_n(z)\} \end{array} \right) \\
&= \max_{\substack{(x-y) \in B_1 \\ (x-z) \in B_2}}^{(k)} \left(\begin{array}{l} \{k \diamond (f(x-y) + \lambda_1(y))\} \cup \{f(x-z) + \mu_1(z)\}, \\ \{k \diamond (f(x-y) + \lambda_2(y))\} \cup \{f(x-z) + \mu_2(z)\}, \\ \dots \\ \{k \diamond (f(x-y) + \lambda_n(y))\} \cup \{f(x-z) + \mu_n(z)\} \end{array} \right) \\
&= \max_{\substack{(x-y) \in B_1 \\ (x-z) \in B_2}}^{(k)} \left[\bigcup_{i=1}^n \{k \diamond (f(x-y) + \lambda_i(y))\} \cup \{f(x-z) + \mu_i(z)\} \right]
\end{aligned}$$



Soft dilation at point $(0, 0)$ for $k = 2$, according to Eq. (38), is

$$\begin{aligned}
 f \oplus [\alpha, \beta, 2](0, 0) &= \max^{(2)}(\{2 \diamond (14, 13)\} \cup \{16, 12, 12, 17\}) \\
 &= \max^{(2)}(14, 14, 13, 13, 16, 12, 12, 17) = 16
 \end{aligned}$$

According to the proposed technique, the structuring is divided into three structuring elements:



The following multisets are obtained from the preceding structuring elements: $\{2 \diamond (14), 16\}$, $\{2 \diamond (13), 12\}$ and $\{12, 17\}$, for the first, the second, and the third structuring elements, respectively. From these multisets the max and $\max^{(2)}$ elements are retained: $\{16, 14\}$, $\{13, 13\}$ and $\{17, 12\}$. The $\max^{(2)}$ of the union of these multisets, i.e., 16, is the result of soft dilation at point $(0, 0)$. It should be noted that although 16 is the max of the first multiset, it is also the $\max^{(2)}$ of the global multiset.

V. FUZZY SOFT MATHEMATICAL MORPHOLOGY

A. Definitions

Fuzzy soft mathematical morphology operations are defined taking into consideration that in soft mathematical morphology the structuring element is divided into two subsets, i.e., the core and the soft boundary, from which the core “weights” more than the soft boundary in the formation of the final result. Also, depending on k , the k th-order statistic provides the result of the operation. Fuzzy soft morphological operation should also preserve the notion of fuzzy fitting (Sinha and Dougherty, 1992). Thus, the definitions for fuzzy soft erosion and fuzzy soft dilation are (Gasteratos *et al.*, 1998a):

$$\mu_{A \ominus [B_1, B_2, k]}(x) = \min[1, \min_{\substack{y \in B_1 \\ z \in B_2}}^{(k)} (\{k \diamond (\mu_A(x + y) - \mu_{B_1}(y) + 1)\} \cup \{\mu_A(x + z) - \mu_{B_2}(z) + 1\})] \quad (59)$$

and

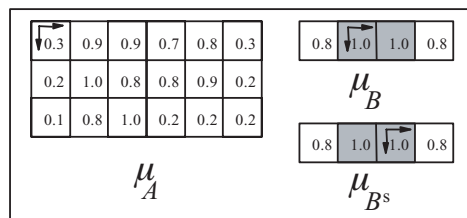
$$\mu_{A \oplus [B_1, B_2, k]}(x) = \max[0, \max_{\substack{(x-y) \in B_1 \\ (x-z) \in B_2}}^{(k)} (\{k \diamond (\mu_A(x-y) + \mu_{B_1}(y) - 1)\} \cup \{\mu_A(x-z) + \mu_{B_2}(z) - 1\})] \quad (60)$$

respectively.

where $x, y, z, \in Z^2$, are the spatial coordinates and $\mu_A, \mu_{B_1}, \mu_{B_2}$ are the membership functions of the image, the core of the structuring element, and the soft boundary of the structuring element. Additionally, for the fuzzy structuring element $B \subset Z^2: B = B_1 \cup B_2$ and $B_1 \cap B_2 = \emptyset$.

It is obvious that for $k = 1$, Eqs. (59) and (60) are reformed to Eqs. (31) and (32), respectively, i.e., standard fuzzy morphology.

Example V.1 Let us consider the image A and the structuring element B . Fuzzy soft erosion and fuzzy soft dilation are computed for cases $k = 1$ and $k = 2$.



In order to preserve the nature of soft morphological operations, the constraint $k \leq \min \{\text{Card}(B)/2, \text{Card}(B_2)\}$ is adopted in fuzzy soft mathematical morphology as well as in soft mathematical morphology. In this example only the cases of $k = 1$ and $k = 2$ are considered, in order to comply with this constraint.

Case 1 ($k = 1$): The fuzzy soft erosion of the image is calculated as follows:

$$\begin{aligned} \mu_E(0, 0) &= \mu_{A \oplus [B_1, B_2, 1]}(0, 0) = \min[1, \min[0.3 - 1 + 1, 0.9 - 1 + 1, 0.9 - 0.8 + 1]] = 0.3 \\ \mu_E(0, 1) &= \min[1, \min[0.3 - 0.8 + 1, 0.9 - 1 + 1, 0.9 - 1 + 1, 0.7 - 0.8 + 1]] = 0.5 \\ &\vdots \\ \mu_E(5, 2) &= \min[1, \min[0.2 - 0.8 + 1, 0.2 - 1 + 1]] = 0.2 \end{aligned}$$

Therefore, the eroded image is:

| | | | | | | |
|---|-----|-----|-----|-----|-----|-----|
| ↓ | 0.3 | 0.5 | 0.7 | 0.5 | 0.3 | 0.3 |
| | 0.2 | 0.4 | 0.8 | 0.4 | 0.2 | 0.2 |
| | 0.1 | 0.3 | 0.2 | 0.2 | 0.2 | 0.2 |

$\mu_{A \ominus [B_1, B_2, 1]}$

The values of the eroded image at points (0, 2) and (1, 2) are higher than the rest values of the image. This agrees with the notion of fuzzy fitting, because the structuring element fits better only at these points than at the rest points of the image. Fuzzy erosion quantifies the degree of structuring element fitting. The larger the number of pixels of the structuring element, the more difficult the fitting. Furthermore, fuzzy soft erosion shrinks the image. If fuzzy image A is considered as a noisy version of a binary image (Sinha and Dougherty, 1992), then the object of interest consists of points (0, 1), (0, 2), (0, 3), (0, 4), (1, 1), (1, 2), (1, 3), (1, 4), (2, 1) and (2, 2), and the rest is the background. By eroding the image with a 4-pixel horizontal structuring element, it would be expected that the eroded image would comprise points (0, 2) and (1, 2). This is exactly what has been obtained.

Similarly, the dilation of the image is calculated as follows:

$$\begin{aligned} \mu_D(0, 0) &= \mu_{A \oplus [B_1, B_2, 1]}(0, 0) \\ &= \max[0, \max[0.3 + 1 - 1, 0.9 + 0.8 - 1]] = 0.7 \\ \mu_D(0, 1) &= \max[0, \max[0.3 + 1 - 1, 0.9 + 1 - 1, 0.9 + 0.8 - 1]] = 0.9 \\ &\vdots \\ \mu_D(5, 2) &= \max[0, \max[0.2 + 0.8 - 1, 0.2 + 1 - 1, 0.2 + 1 - 1]] = 0.2 \end{aligned}$$

Therefore, the dilated image is:

| | | | | | | |
|---|-----|-----|-----|-----|-----|-----|
| ↓ | 0.7 | 0.9 | 0.9 | 0.9 | 0.8 | 0.8 |
| | 0.8 | 1.0 | 1.0 | 0.8 | 0.9 | 0.9 |
| | 0.6 | 0.8 | 1.0 | 1.0 | 0.8 | 0.2 |

$\mu_{A \oplus [B_1, B_2, 1]}$

As it can be seen, fuzzy soft dilation expands the image. In other words the dilated image includes the points of the original image and also the points (0, 0), (0, 5), (1, 0), (1, 5), (2, 0), (2, 3) and (2, 4).

30 M. I. VARDAVOULIA, A. GASTERATOS, AND I. ANDREADIS

Case 2 ($k=2$): The erosion of the image is calculated as follows:

$$\mu_E(0, 0) = \mu_{A \ominus [B_1, B_2, 2]}(0, 0) = \min [1, \min^{(2)}[0.3, 0.3, 0.9, 0.9, 1.1]] = 0.3$$

$$\mu_E(0, 1) = \min [1, \min^{(2)}[0.5, 0.9, 0.9, 0.9, 0.9, 0.9]] = 0.9$$

⋮

$$\mu_E(5, 2) = \min [1, \min^{(2)}[0.4, 0.2, 0.2]] = 0.2$$

The eroded image for $k=2$ is:

| | | | | | | |
|---------------------------------|-----|-----|-----|-----|-----|-----|
| ↖ | 0.3 | 0.9 | 0.7 | 0.7 | 0.3 | 0.3 |
| ↓ | 0.2 | 0.8 | 0.8 | 0.8 | 0.2 | 0.2 |
| ↘ | 0.1 | 0.4 | 0.2 | 0.2 | 0.2 | 0.2 |
| $\mu_{A \ominus [B_1, B_2, 2]}$ | | | | | | |

In this case the values of the eroded image at points $(0, 1)$, $(0, 2)$, $(0, 3)$, $(1, 1)$, $(1, 2)$ and $(1, 3)$ are higher than the rest values of the image. This is in agreement with the notion of fuzzy soft fitting. At these points the k repeated “high-value” pixels, which are combined with the core of the structuring element, and the pixels that are combined with the soft boundary of the structuring element are greater than or equal to $k \text{Card}[B_1] + \text{Card}[B_2] - k + 1$.

Similarly, the dilation of the image is calculated:

$$\mu_D(0, 0) = \mu_{A \oplus [B_1, B_2, 2]}(0, 0) = \max [0, \max^{(2)}[0.3, 0.3, 0.7]] = 0.3$$

$$\mu_D(0, 1) = \max [0, \max^{(2)}[0.3, 0.3, 0.9, 0.9, 0.7]] = 0.9$$

⋮

$$\mu_D(5, 2) = \max [0, \max^{(2)}[0.4, 0.2, 0.2, 0.2, 0.2]] = 0.2$$

Therefore, the dilated image for $k=2$ is:

| | | | | | | |
|--------------------------------|-----|-----|-----|-----|-----|-----|
| ↖ | 0.3 | 0.9 | 0.9 | 0.9 | 0.8 | 0.8 |
| ↓ | 0.2 | 1.0 | 1.0 | 0.8 | 0.9 | 0.9 |
| ↘ | 0.1 | 0.8 | 1.0 | 1.0 | 0.2 | 0.2 |
| $\mu_{A \oplus [B_1, B_2, 2]}$ | | | | | | |

Here again fuzzy soft dilation expands the image, but more softly than when $k = 1$. This means that certain points $((0, 0), (1, 0), (2, 0), \text{ and } (2, 4))$, which were considered image points (when $k = 1$, now $k = 2$), belong to the background. The greater the value of k , the less the effect of dilation.

Finally, fuzzy soft opening and closing are defined as

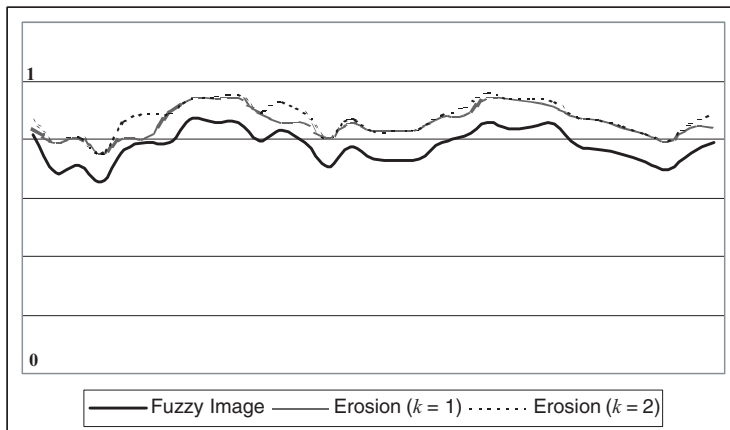
$$\mu_{A \circ [B_1, B_2, k]}(x) = \mu_{(A \ominus [B_1, B_2, k]) \oplus [B_1, B_2, k]}(x) \quad \text{and} \quad (61)$$

$$\mu_{A \bullet [B_1, B_2, k]}(x) = \mu_{(A \oplus [B_1, B_2, k]) \ominus [B_1, B_2, k]}(x) \quad (62)$$

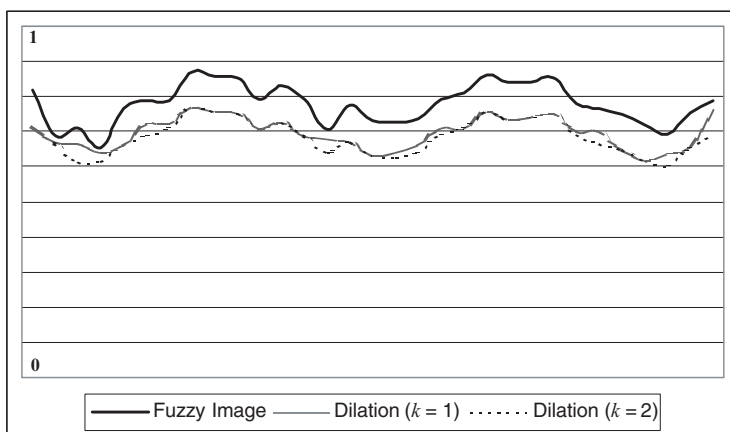
respectively.

Illustration of the basic fuzzy soft morphological operations is given through one-dimensional and two-dimensional signals. Figure 5 depicts fuzzy soft morphological erosion and dilation in one-dimensional space. More specifically, Figure 5a shows the initial one-dimensional signal and fuzzy soft erosion for $k = 1$ and for $k = 2$. Figure 5b shows the initial one-dimensional signal and fuzzy soft dilation for $k = 1$ and for $k = 2$. Figure 5c shows the structuring element. The core of the structuring element is the shaded area, and the rest area of the structuring element is its soft boundary. From Figures 5a and 5b it becomes clear that the action of the structuring element becomes more effective when $k = 1$, i.e., the results of both fuzzy soft erosion and dilation are more visible in the case of $k = 1$ than in the case of $k = 2$. Moreover, both erosion and dilation preserve the details of the original image better in the case of $k = 2$ than in the case of $k = 1$.

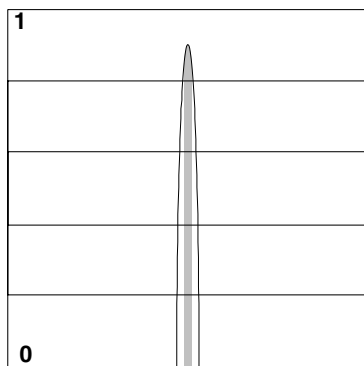
Figure 6 presents the result of fuzzy soft morphological erosion and dilation on a two-dimensional image. More specifically, Figures 6a and 6b present the initial image and the structuring element, respectively. The image in Figure 6b has been considered as an array of fuzzy singletons (Goetcharian, 1980). The results of fuzzy soft erosion ($k = 1$) after the first and second interactions are presented in Figures 6c and 6d, respectively. The white area is reduced after each interaction. The white area of the eroded image (Figure 6c) is the area of the initial image, where the structuring element fits better. Similarly, Figures 6e and 6f present the results of fuzzy soft erosion ($k = 3$) after the first and second interaction, respectively. Comparing Figures 6c and 6e, it becomes clear that the greater k is, the less visible are the results of fuzzy soft erosion. Figures 6g and 6h depict the results of fuzzy soft dilation ($k = 1$) after the first and second interactions, respectively. In the case of fuzzy soft dilation, the white area increases. Similarly, Figures 6i and 6j show the results of fuzzy soft dilation ($k = 3$) after the first and the second interaction, respectively. Again, the greater k is, the less visible are the results of fuzzy soft dilation.



(a)



(b)



(c)

FIGURE 5. Illustration of one-dimensional fuzzy soft morphological operations and the effect of the order index k : (a) fuzzy soft erosion, (b) a fuzzy soft dilation, and (c) the structuring element.

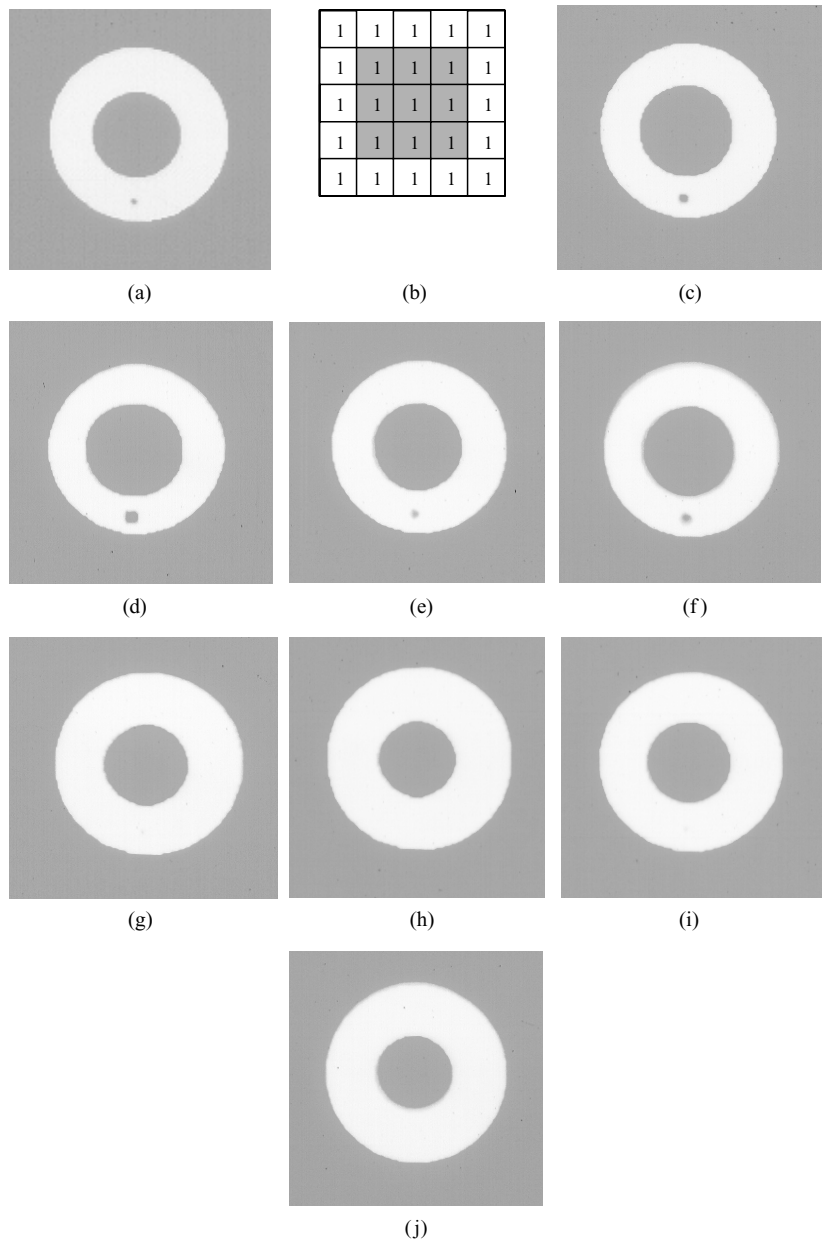
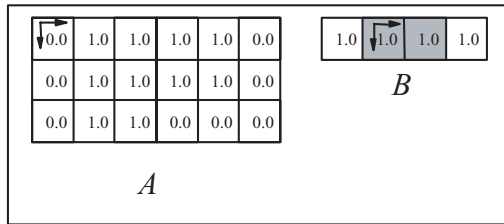


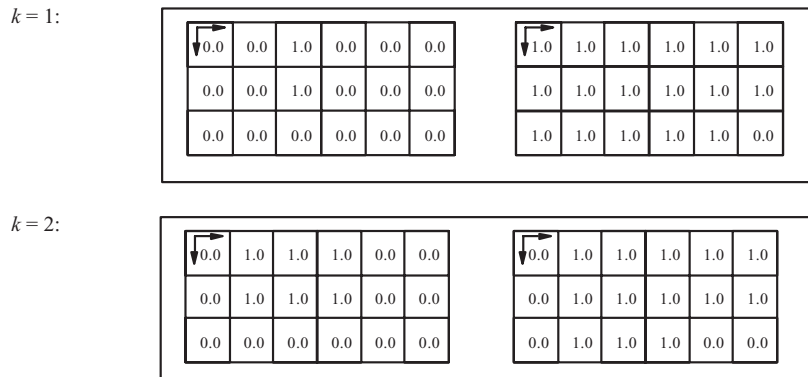
FIGURE 6. (a) Image, (b) structuring element, (c) fuzzy soft erosion ($k = 1$) after the first interaction, (d) fuzzy soft erosion ($k = 1$) after the second interaction, (e) fuzzy soft erosion ($k = 3$) after the first interaction, (f) fuzzy soft erosion ($k = 3$) after the second interaction, (g) fuzzy soft dilation ($k = 1$) after the first interaction, (h) fuzzy soft dilation ($k = 1$) after the second interaction, (i) fuzzy soft dilation ($k = 3$) after the first interaction, and (j) fuzzy soft dilation ($k = 3$) after the second interaction.

B. Compatibility with Soft Mathematical Morphology

Let us consider Example V.I. By thresholding image *A* and structuring element *B* (using a threshold equal to 0.5), the following binary image and binary structuring element are obtained:



By applying soft binary erosion and soft binary dilation to image *A* with structuring element *B*, the following images are obtained for $k=1$ and $k=2$:



It is obvious that these results are identical to those of Example V.1, when the same threshold value is used. This was expected, because binary soft morphology quantifies the soft fitting in a crisp way, whereas fuzzy soft erosion quantifies the soft fitting in a fuzzy way. The same results are obtained using a threshold equal to 0.55. However, when fuzzy soft morphology and thresholding with a threshold equal to or greater than 0.6 on the one hand and thresholding with the same threshold and soft morphology on the other hand are applied, different results will be obtained. This means that, in general, the operations do not commute.

C. Algebraic Properties of Fuzzy Soft Mathematical Morphology

Theorem V.1 Duality Theorem

Fuzzy soft erosion and dilation are dual operations:

$$\mu_{A^c \oplus [B_1, -B_2, k]}(x) = \mu_{(A \ominus [B_1, B_2, k])^c}(x) \tag{63}$$

Opening and closing are also dual operations:

$$\mu_{(A \bullet [B_1, B_2, k])^c}(x) = \mu_{A^c \circ [-B_1, -B_2, k]}(x) \tag{64}$$

Theorem V.2 Translation Invariance

Fuzzy soft erosion and dilation are translation invariant:

$$\mu_{(A)_u \ominus [B_1, B_2, k]}(x) = (\mu_{A \ominus [B_1, B_2, k]}(x))_u \tag{65}$$

where $u \in \mathbb{Z}^2$.

Theorem V.3 Increasing Operations

Both fuzzy soft erosion and dilation are increasing operations:

$$\mu_A < \mu_{A'} \Rightarrow \begin{cases} \mu_{A \ominus [B_1, B_2, k]}(x) < \mu_{A' \ominus [B_1, B_2, k]}(x) \\ \mu_{A \oplus [B_1, B_2, k]}(x) < \mu_{A' \oplus [B_1, B_2, k]}(x) \end{cases} \tag{66}$$

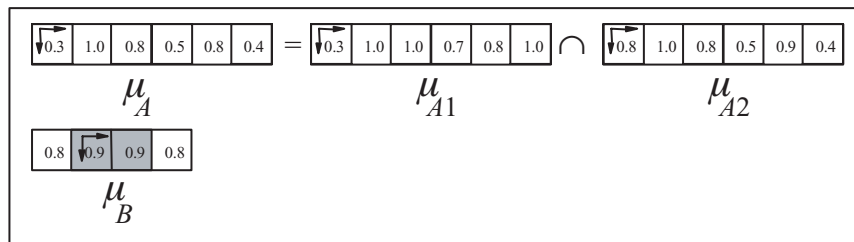
where A and A' , are two images with membership functions μ_A and $\mu_{A'}$, respectively and $\mu_A(x) < \mu_{A'}(x), \forall x \in \mathbb{Z}^2$.

Theorem V.4 Distributivity

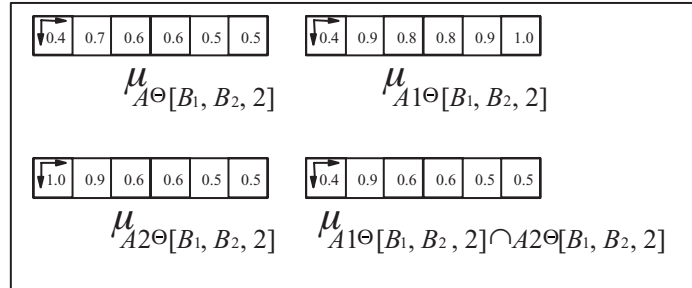
Fuzzy soft erosion is not distributive over intersection, as it is in standard morphology:

$$\exists x \in \mathbb{Z}^2 \text{ and } \exists A_1, A_2, B \subseteq \mathbb{Z}^2 | \mu_{(A_1 \cap A_2) \ominus [B_1, B_2, k]}(x) \neq \mu_{(A_1 \ominus [B_1, B_2, k]) \cap (A_2 \ominus [B_1, B_2, k])}(x) \tag{67}$$

Example V.2 Consider the following image A and structuring element B , where image A is the intersection of images A_1 and A_2 .



The fuzzy soft erosion for $k = 2$ of $A, A1, A2$ and the intersection of the eroded $A1$ and the eroded $A2$ are:



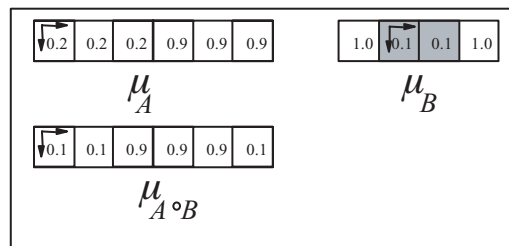
In general, fuzzy soft dilation does not distribute over union:

$$\exists x \in Z^2 \quad \text{and} \quad \exists A1, A2, B \subseteq Z^2 \mid \mu_{(A1 \cup A2) \oplus [B_1, B_2, k]}(x) \neq \mu_{(A1 \oplus [B_1, B_2, k]) \cup (A2 \oplus [B_1, B_2, k])}(x) \quad (68)$$

Theorem V.5 *Antiextensivity–Extensivity*

Fuzzy soft opening is not antiextensive. If it were antiextensive, then $\mu_{A \circ [B_1, B_2, k]}(x) \leq \mu_A(x), \forall x \in Z^2$. The following example shows that $\exists x \in Z^2 \mid \mu_{A \circ [B_1, B_2, k]}(x) > \mu_A(x)$.

Example V.3 Consider the image A and the structuring element B for $k = 2$. In this example



$$\mu_{A \circ [B_1, B_2, k]}(0, 2) = 0.9 > \mu_A(0, 2) = 0.2$$

which means that fuzzy soft opening is not antiextensive.

Similarly, it can be shown that, in general, fuzzy soft closing is not extensive: $\exists x \in Z^2$ and $A, B \subseteq Z^2 \mid \mu_{A \bullet [B_1, B_2, k]}(x) < \mu_A(x)$.

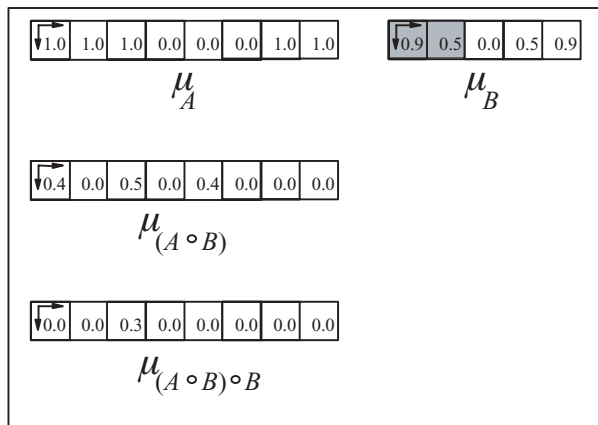
Theorem V.6 *Idempotency*

In general, fuzzy soft opening is not idempotent:

$$\exists x \in Z^2 \quad \text{and} \quad \exists A, B \subseteq Z^2 \mid \mu_{A \circ [B_1, B_2, k]}(x) \neq \mu_{(A \circ [B_1, B_2, k]) \circ [B_1, B_2, k]}(x) \quad (69)$$

This is illustrated by the following example.

Example V.4 Consider the image A and the structuring element B for $k = 1$.



From this example it is obvious that fuzzy soft opening is not idempotent.

By the duality theorem (Eq. (64)) it can be proved that, in general, fuzzy soft closing is also not idempotent:

$$\exists x \in Z^2 \quad \text{and} \quad \exists A, B \subseteq Z^2 \mid \mu_{A \bullet [B_1, B_2, k]}(x) \neq \mu_{(A \bullet [B_1, B_2, k]) \bullet [B_1, B_2, k]}(x) \quad (70)$$

VI. IMPLEMENTATIONS

Soft morphological operations are based on weighted order statistics and, therefore, algorithms such as mergesort and quicksort, which were developed for the computation of weighted order statistics, can be used for the computation of soft morphological filters (Kuusmanen and Astola, 1995). The average complexity of the quicksort algorithm is $O(N \log N)$, where N is the number of elements to be sorted (Pitas and Venetsanopoulos, 1990). Therefore, the average complexity for a soft morphological operation utilizing a soft structuring element $[\alpha, \beta, k]: B \rightarrow Z$ is $O((k \text{ Card}[B_1] + \text{Card}[B_2]) \log(k \text{ Card}[B_1] + \text{Card}[B_2]))$.

Hardware implementations of soft morphological operations include the threshold decomposition and the majority gate techniques. These structures, along with an algorithm based on a local histogram, are described in some detail in this section.

A. Threshold Decomposition

The threshold decomposition (Wendt *et al.*, 1985) is a well-known technique for hardware implementation of nonlinear filters. The implementation of soft morphological filters in hardware, using the threshold decomposition technique, has been described in Shih and Pu (1995) and Pu and Shih (1995). According to this approach, both the gray-scale image and the gray-scale structuring element are decomposed into 2^b binary images f_i and 2^b structuring elements β_i , respectively. Binary soft morphological operations are performed on the binary images by the binary soft structuring elements and then a maximum or a minimum selection at each position is performed, depending whether the operation is soft dilation or soft erosion, respectively. Finally, the addition of the corresponding binary pixels is performed. Figure 7 demonstrates this technique for soft dilation.

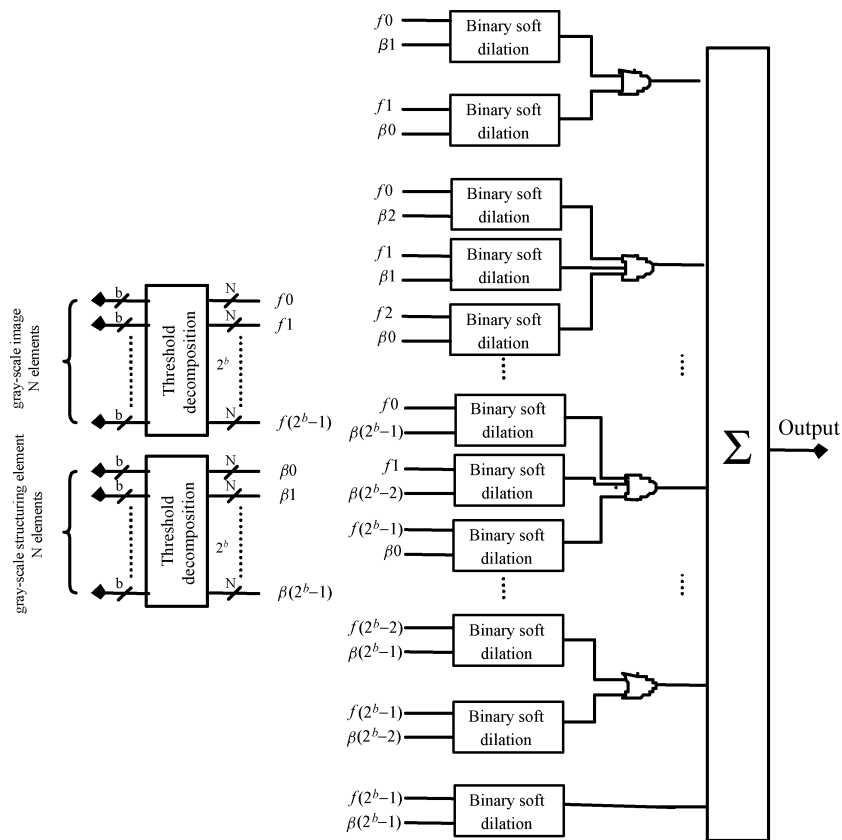


FIGURE 7. Illustration of the threshold decomposition technique for soft dilation.

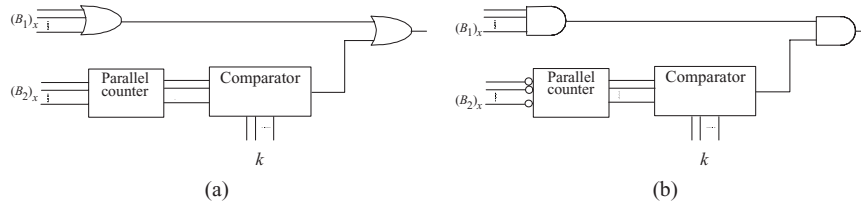


FIGURE 8. Implementation of binary (a) soft morphological dilation and (b) soft morphological erosion.

The logic-gate implementation of binary soft morphological dilation and erosion are shown in Figures 8a and 8b, respectively. The parallel counter counts the number of 1s of the input signal and the comparator compares them to the order index k and outputs 1 when this number is greater than or equal to k .

It is obvious that this technique, although it can achieve high-speed computation times, is hardware demanding because it is realized using simple binary structures. Its hardware complexity grows exponentially both with the structuring element size and the resolution of the pixels, i.e., its hardware complexity is $O(2^N 2^b)$.

B. Majority Gate

1. Algorithm Description

The majority gate algorithm is an efficient bit serial algorithm suitable for the computation of the median filter (Lee and Jen, 1992). According to this algorithm, the MSBs of the numbers within the data window are first processed. The other bits are then processed sequentially until the less significant bits (LSBs) are reached. Initially, a set of signals (named the rejecting flag signals) are set to 1. These signals indicate which numbers are candidates to be the median value. If the majority of the MSBs are found to be 1s, then the MSB of the output is 1; otherwise, it is 0. The majority is computed through a CMOS programmable device, shown in Figure 9. In the following stage the bits of the numbers whose MSBs have been rejected by means of the rejecting flag signals are not taken into account. The majority selection procedure continues in the next stages until the median value is found.

Gasteratos *et al.* (1997a) have proposed an improvement of this algorithm for the implementation of any rank filter using a single hardware structure. This is based on the concept that by having a method to compute the median value of $4N + 1$ numbers and by being able to control $2N$ of these numbers,

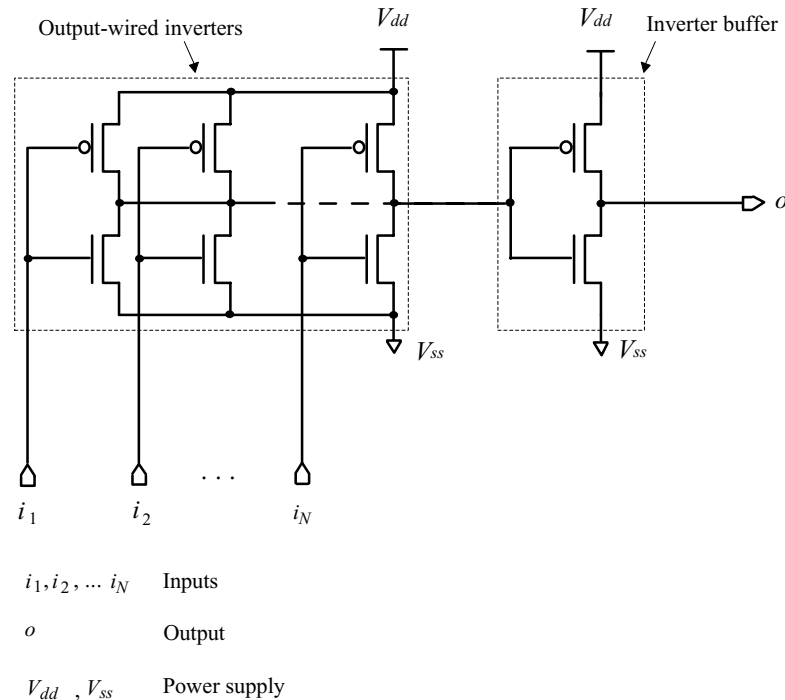


FIGURE 9. Programmable CMOS majority gate.

any order statistic of the rest $2N + 1$ numbers can be determined. Suppose that there are $W = 2N + 1$ numbers x_i , the r th-order statistic of which is required. The $2N + 1$ inputs are the numbers x_i , whereas the rest are dummy inputs d_i ($0 < i \leq 2N$). The binary values of the dummy inputs can be either $00 \dots 0$ or $11 \dots 1$. This implies that when the W numbers are ordered in ascending sequence, d_i are placed to the extremes of this sequence.

2. Systolic Array Implementation for Soft Morphological Filtering

2a. A Systolic Array for a 3×3 Structuring Element

A pipelined systolic array capable of computing soft gray-scale dilation/erosion on a 3×3 -pixel image window using a 3×3 -pixel structuring element, both of 8-bit resolution, is presented in Figure 10 (Gasteratos *et al.*, 1998b). The central pixel of the structuring element is its core, whereas the other eight pixels constitute its soft boundary. The inputs to this array are the nine pixels of the image window and the nine pixels of the soft morphological structuring element and a control signal MODE. Latches (L1) store the image window,

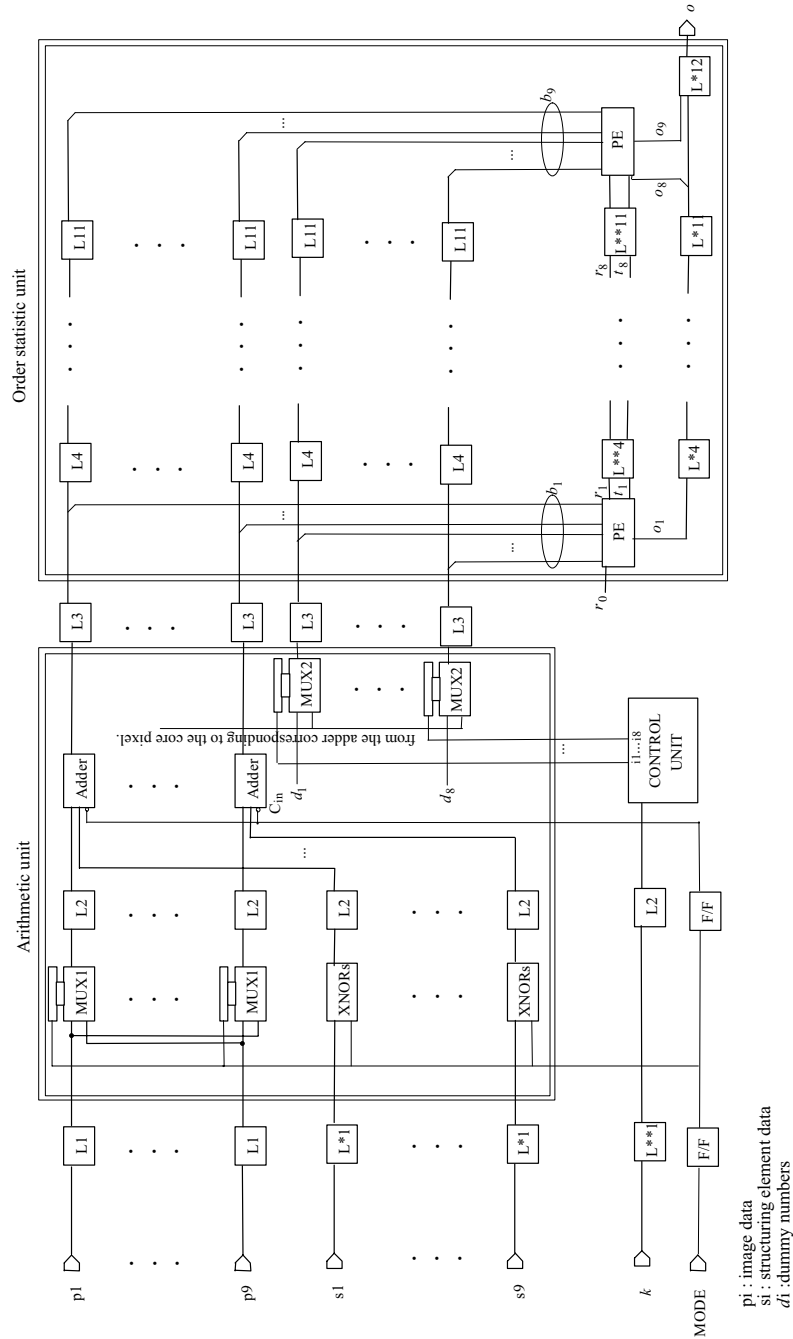


FIGURE 10. Systolic array hardware structure implementing the majority gate technique for soft morphological filtering.

TABLE 1
USE OF DUMMY NUMBERS IN THE COMPUTATION OF WEIGHT
ORDER STATISTICS

| k | Sequence of numbers | Dummy numbers |
|-----|---------------------|---------------|
| 1 | 9 | 8 |
| 2 | 10 | 7 |
| 3 | 11 | 6 |
| 4 | 12 | 5 |

latches ($L*1$) store the structuring element, and latch ($L**1$) stores the number k . Signal MODE is used to select the operation. When this is 1, soft dilation is performed, whereas when it is 0, a soft erosion operation is performed. Image data are collected through multiplexers MUX1, which are controlled by the signal MODE. The pixels of the structuring element remain either unchanged for the operation of dilation or they are complemented (by means of XNOR gates) for the operation of erosion. In the next stage of the pipeline, data are fed into nine adders. In the case of soft erosion, the 2's complements of the pixel values of the structuring element are added to the image pixel values. This is equivalent to the subtraction operation.

According to the constraint $k \leq \min\{\text{Card}(B)/2, \text{Card}(B_2)\}$, in this case k is in the range $1 \leq k \leq 4$. Table 1 shows the number of the elements of the image data window contained in the list, as well as the number of the dummy elements. For soft dilation all the dummy inputs are pushed to the top, whereas for soft erosion they are pushed to the bottom. Thus, the appropriate result is obtained from the order statistic unit. A control unit controls an array of multiplexers MUX2 (its input is number k). This is a decoder, and its truth table is shown in Table 2. It provides the input to the order statistic unit, either a dummy number or a copy of the addition/subtraction result of the core.

TABLE 2
TRUTH TABLE OF THE CONTROL UNIT

| Input k | Outputs | | | | | | | |
|--------------|---------|----|----|----|----|----|----|----|
| | i1 | i2 | i3 | i4 | i5 | i6 | i7 | i8 |
| 0001 | 0 | 0 | 0 | 0 | 0 | 0 | 0 | 0 |
| 0010 | 1 | 0 | 0 | 0 | 0 | 0 | 0 | 0 |
| 0011 | 1 | 1 | 0 | 0 | 0 | 0 | 0 | 0 |
| 0100 | 1 | 1 | 1 | 0 | 0 | 0 | 0 | 0 |

The order statistic unit consists of identical processing elements (PEs) separated by latches ($L^{**}4$ to $L^{**}11$). The resolution of the latches, which hold the addition/subtraction results or the dummy numbers ($L3$ to $L11$), decreases by 1 bit at each successive stage, because there is no need to carry the bits, which have been already processed. On the other hand, the resolution of the latches that hold the result ($L4^*$ to $L^{*}11$), increases by 1 bit at each successive stage. The circuit diagram of this PE is shown in Figure 11. In this figure $W' = 4N + 1$; the $2N + 1$ inputs are the numbers x_i , whereas the rest

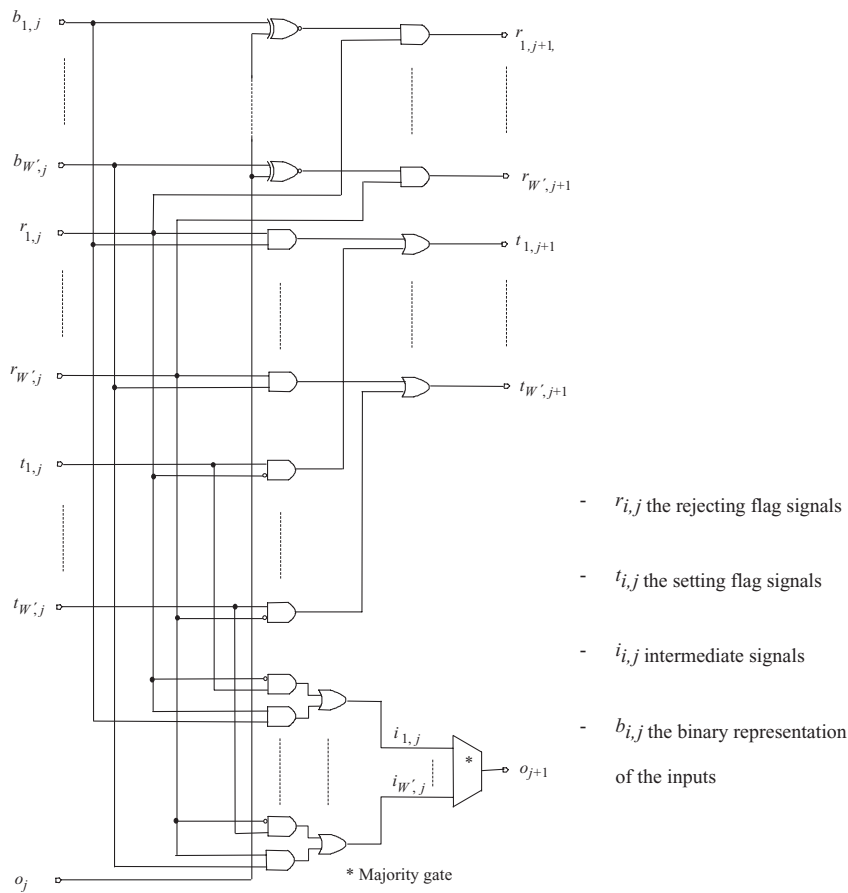


FIGURE 11. The basic processing element (PE).

are the dummy inputs. Due to its simplicity, it can attain very short processing times, independent of the data window size. Also, it becomes clear that the hardware complexity of the PE is linearly related to the number of its inputs.

2b. Order Statistic Module Hardware Requirements for Other Structuring Elements

In the next describe a case study of the hardware requirements for the order statistic unit of a more complex structuring element. The arithmetic unit consists of a number of adders/subtractors equal to the number of pixels of the structuring element. Figure 12a illustrates the structuring element. In this case: $\text{Card}(B) = 16$, $\text{Card}(B_1) = 12$, $\text{Card}(B_2) = 4$, and $k \leq \min\{8, 4\}$, i.e., $1 \leq k \leq 4$. When $k = 4$ the maximum number of the elements of the multiset is $\text{Card}(B_2) + k \text{Card}(B_1) = 52$. The 49th- (4th-) order statistic of the multiset is sought. Thus, the total number of the inputs to the order statistic unit is 97. The dummy numbers, which are pushed to the top (bottom) in the operation of soft dilation (erosion), are 45. When $k = 3$, the elements of the multiset are 40 and the 38th- (3rd-) order statistic is searched. Now the dummy numbers, which are pushed to the top (bottom), are 46 and to the bottom (top) are 11. In the same way, when $k = 2$ the elements of the multiset are 28 and the 27th- (2nd-) order statistic is searched and the dummy numbers that are pushed to the top (bottom) are 47 and to the bottom (top) are 22. Finally, when $k = 1$ the elements of the multiset are 16 and the 16th- (1st-) order statistic is searched. In this case the dummy numbers that are pushed to the top (bottom) are 48 and to the bottom (top) are 33. For any structuring element, an order statistic unit can be synthesized following this procedure. In this case hardware complexity is linearly related both to the structuring element size and the resolution of the pixels, i.e., the hardware complexity is $O(Nb)$.

3. Architecture for Decomposition of Soft Morphological Structuring Elements

An architecture suitable for the decomposition of soft morphological structuring elements is depicted in Figure 13. The structuring element is loaded into the *structuring element management* module. This divides the structuring element into n smaller structuring elements and provides the appropriate one to the next stage. The pixels of the image are imported into the *image window-management* module. This provides an image window, which interacts with the appropriate structuring element, provided by the *structuring element-management* module. Both the previous modules consist of registers

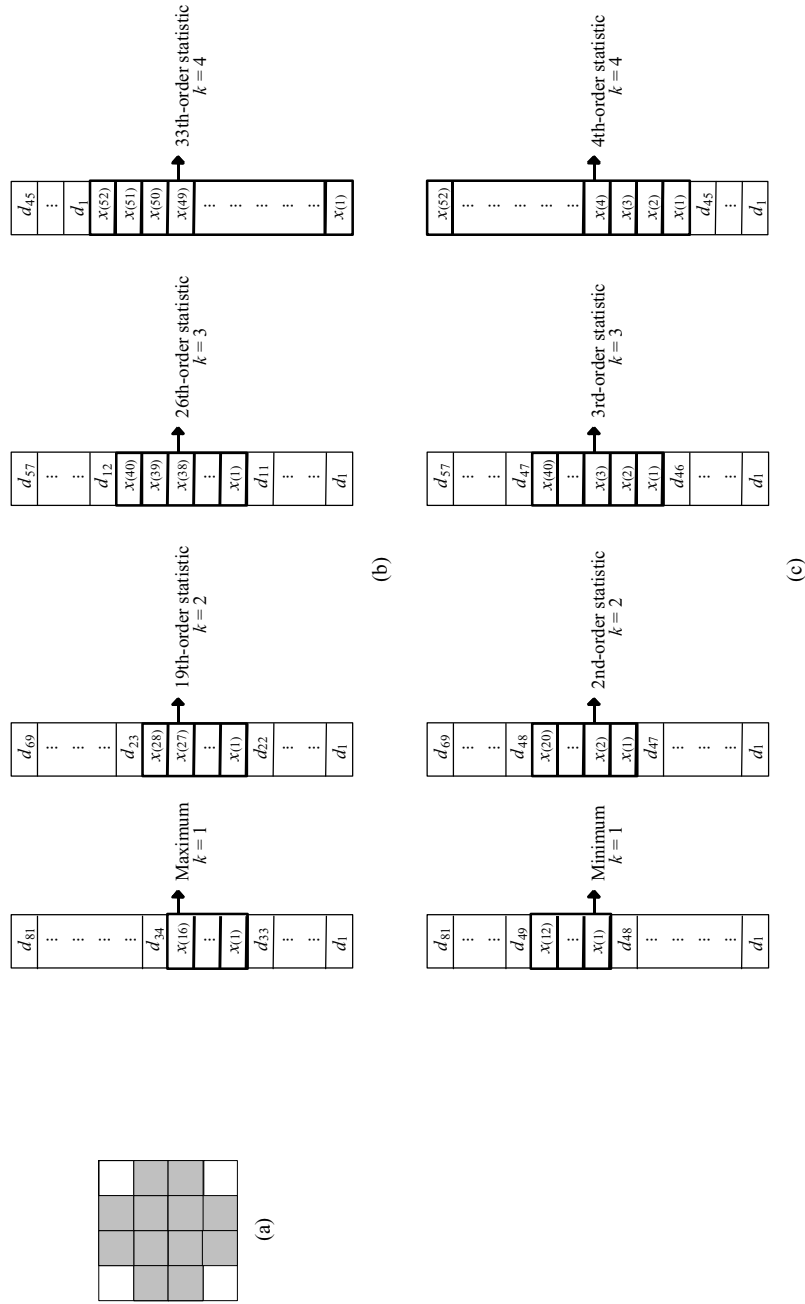


FIGURE 12. (a) Structuring element, (b) arrangement of the dummy numbers in soft morphological dilation using the structuring element of $k=1$, and (c) arrangement of the dummy numbers in soft morphological erosion using the same structuring element.

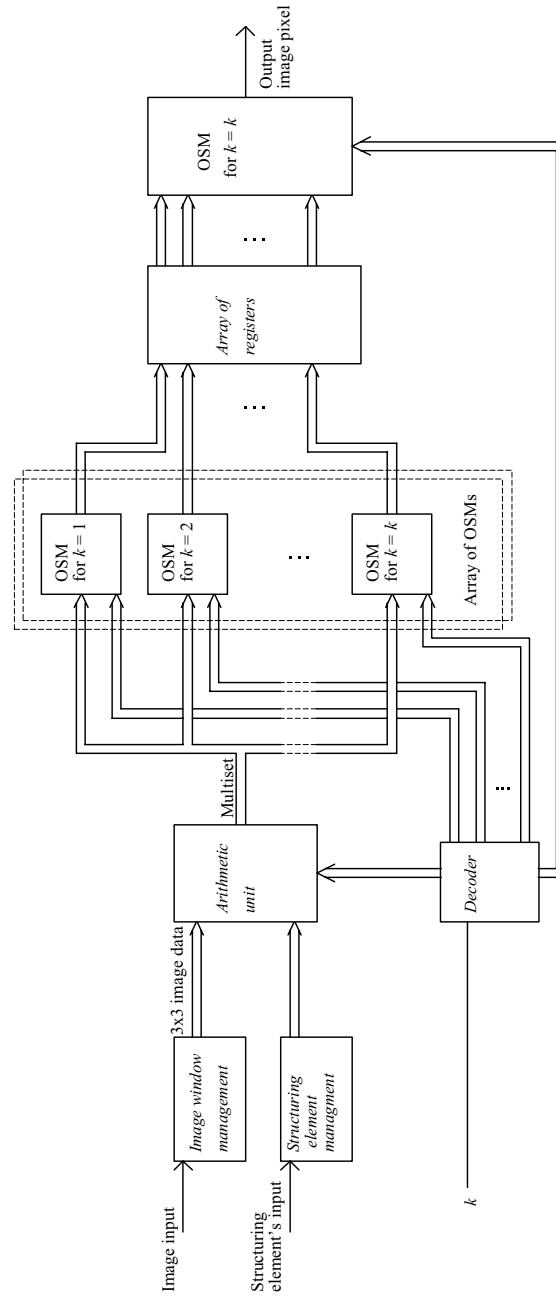


FIGURE 13. Architecture for the implementation of the soft morphological structuring element decomposition technique.

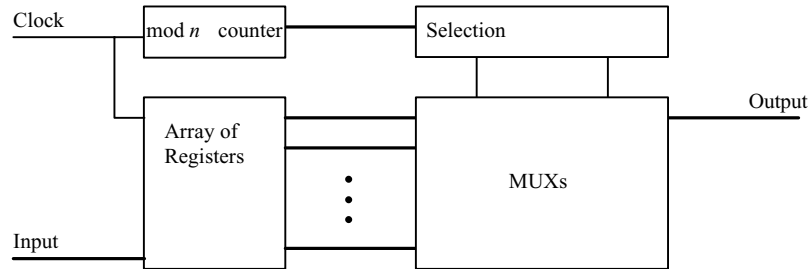


FIGURE 14. Data window management for soft morphological structuring element decomposition.

and multiplexers (MUXs), controlled by a counter mod n (Fig. 14). The second stage, i.e., the *arithmetic unit*, consists of adders/subtractors (dilation/erosion) and an array of MUXs that are controlled by the order index k , as the one shown in Figure 11. The MUXs provide the multiple copies of the addition/subtraction results to the next stage, i.e., an array of *order statistic modules* (OSMs). The $\max^{(l)}/\min^{(l)}$ results ($l = 1, \dots, k$) of every multiset are collected through an *array of registers*. These registers provide the $n \times k$ $\max^{(l)}/\min^{(l)}$ of the n multisets concurrently to the last stage OSM, which computes the final result according to Eqs. (55) and (56).

C. Histogram Technique

A method for computing an order statistic is to sum the values in the local histogram until the desired order statistic is reached (Dougherty and Astola, 1994). However, instead of adding the local histogram values serially, a successive approximation technique can be adopted (Gasteratos and Andreadis, 1994). This ensures that the result is traced in a fixed number of steps. The number of steps is equal to the number b of the bits per pixel. In the successive approximation technique the result is computed recursively; in each step of the process the N pixel values are compared to a temporal result. Pixel values, which are greater than, less than, or equal to that temporal result, are marked with labels GT, LT, and EQ, respectively. GT, LT and EQ are Boolean variables. Pixel labels are then multiplied by the corresponding pixel weight (w_j). The sum of LTs and EQs determines whether the k th-order statistic is greater than, less than, or equal to the temporal values.

The pseudocode of the algorithm follows:

48 M. I. VARDAVOULIA, A. GASTERATOS, AND I. ANDREADIS

Notation: N : number of pixels; b : pixel value resolution (bits); im_1, im_2, \dots, im_N : image pixels; w_1, w_2, \dots, w_N : corresponding weights; k : the sought order statistic; temp: temporal result; o : output pixel.

```

initial
 $o = 0$ 
 $temp = 2^{b-1}$ 
begin
for  $i = 1$  to  $b$  do
  begin
  compare( $im_1, im_2, \dots, im_N$ : temp)
  {if  $im_j = temp$  then  $EQ_j = 1$  else  $EQ_j = 0$ 
  if  $im_j < temp$  then  $LT_j = 1$  else  $LT_j = 0$ }
  if  $\left( \sum_{j=1}^N w_j(EQ_j + LT_j) \geq k \right)$  AND  $\left( \sum_{j=1}^N w_j LT_j < k \right)$ 
  then  $o \leftarrow temp$ 
  elseif  $\sum_{j=1}^N w_j LT_j \geq k$ 
  then  $temp \leftarrow temp - 2^{b-1-i}$ 
  else  $temp \leftarrow temp + 2^{b-1-i}$ 
  end
end

```

A module utilizing standard comparators, adders/subtractors, multipliers, and multiplexers (for the “if” operations) can be used to implement this technique in hardware. Also, there are two ways to realize the algorithm. The first is through a loop, which feeds the temp signal back to the input b times. Such a module is demonstrated in Figure 15. Its inputs are the addition or subtraction results of the image pixel value data with the structuring element pixel values, depending on whether the operation is soft dilation or soft erosion, respectively. Alternatively, b successive modules can be used to process the data in a pipeline fashion. The latter implementation is more hardware demanding but results in a faster hardware structure.

The preceding algorithm requires a fixed number of steps equal to b . Furthermore, the number of steps grows linearly according to the pixel value resolution ($O(b)$). Its main advantage is that it can directly compute weighted rank order operations. This means that there is no need to reconstruct the local histogram according to the weights of the image pixels. Comparative experimental results using typical images showed that for 5×5 and larger image data windows the combined local histogram and successive approximation technique outperforms the existing quicksort algorithm for weighted order statistics filtering (Gasteratos and Andreadis, 1999).

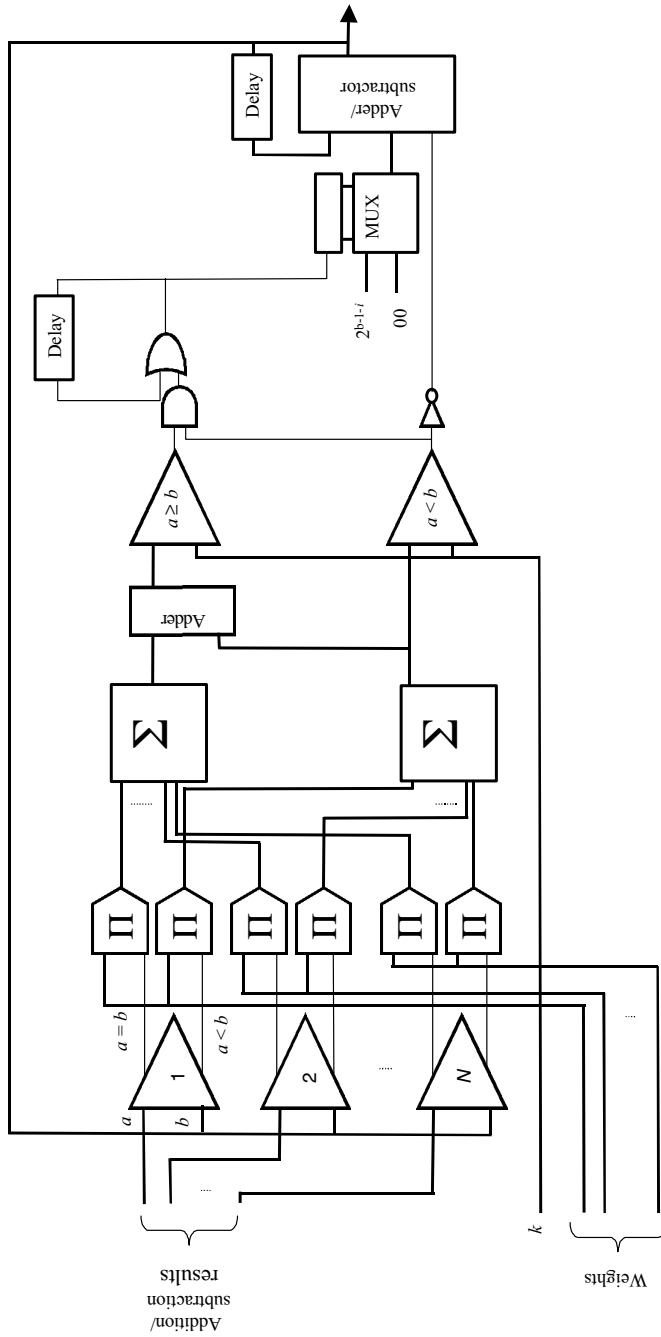


FIGURE 15. Block diagram of a hardware module for the computation of weighted order statistics, based on the local histogram-successive approximation technique.

D. Vector Standard Morphological Operation Implementation

The block diagram of a new hardware structure that performs vector erosion or dilation of a color image f by a color 3×3 -pixel structuring element g , both of 24-bit resolution, is presented in Figure 16. The input image f may be of any dimension. Consider that the 3×3 -pixel window defined by the domain G of g is located at spatial coordinates x , including the nine vectors of the input image, $vecim_j$ ($1 \leq j \leq 9$). In each clock cycle the j th vector of the input image ($vecim_j$) and the corresponding j th vector of the structuring element ($vecse_j$) are imported into the input unit. This unit consists of an array of D-type flip-flops and a MUX, which ensures that after the ninth clock cycle the nine vectors of the structuring element are feedback to the input unit. Thus, the structuring element is introduced only once.

In Figure 16 we assume that $vecim_j = c(him_j, sim_j, vim_j)$ and also $vecim_j = c(him_j, sim_j, vim_j)$. As can be seen, in the next clock cycle the h , s , and v components of the j th vectors under consideration are pairwise subtracted or added in the summation/subtraction units, according to the value of the select operation input signal, which determines the vector morphological operation (erosion or dilation) that is carried out.

In the next stage, the h , s , and v differences or sums are normalized to the upper or the lower bound of each vector component (see constraints in Eqs. (29) and (30)) in the three normalization units. These three differences or sums are the components of the j th vector ($vector_j$) in $\{f(x+y) - g(y)\}$ or in $\{f(x-y) + g(y)\}$, respectively (see Eqs. (27) and (28)).

Consequently, $vector_j$ is loaded into the supremum or infimum finding module. The heart of this module is a mod-9 counter, which ensures that the nine vectors in $\{f(x+y) - g(y)\}$ or in $\{f(x-y) + g(y)\}$ will be compared during nine clock cycles and the infimum or the supremum of these nine vectors will be the output of the module at the tenth clock cycle. The module also includes an array of D-type flip-flops, which transmit the j th and the $(j+1)$ st vectors ($vector_j$ and $vector_{j+1}$) simultaneously to an array of comparators (each comparator of the array compares only one component of the vectors under consideration). The outputs of the comparators are then fed to the control unit (a combinational circuit), which, according to the select operation signal, determines whether the j th or the $(j+1)$ st vector will be compared to the next input of the module, i.e., the $(j+2)$ nd vector ($vector_{j+2}$). The result of the ninth comparison is forwarded to the output of the module, through an array of MUXs.

The whole procedure is fully pipelined. After initialization, the hardware structure of Figure 16 produces an output result every nine clock cycles.

The proposed circuit was designed and successfully simulated by means of the MAX+plus II software of Alter a Corporation. The FPGA used is the

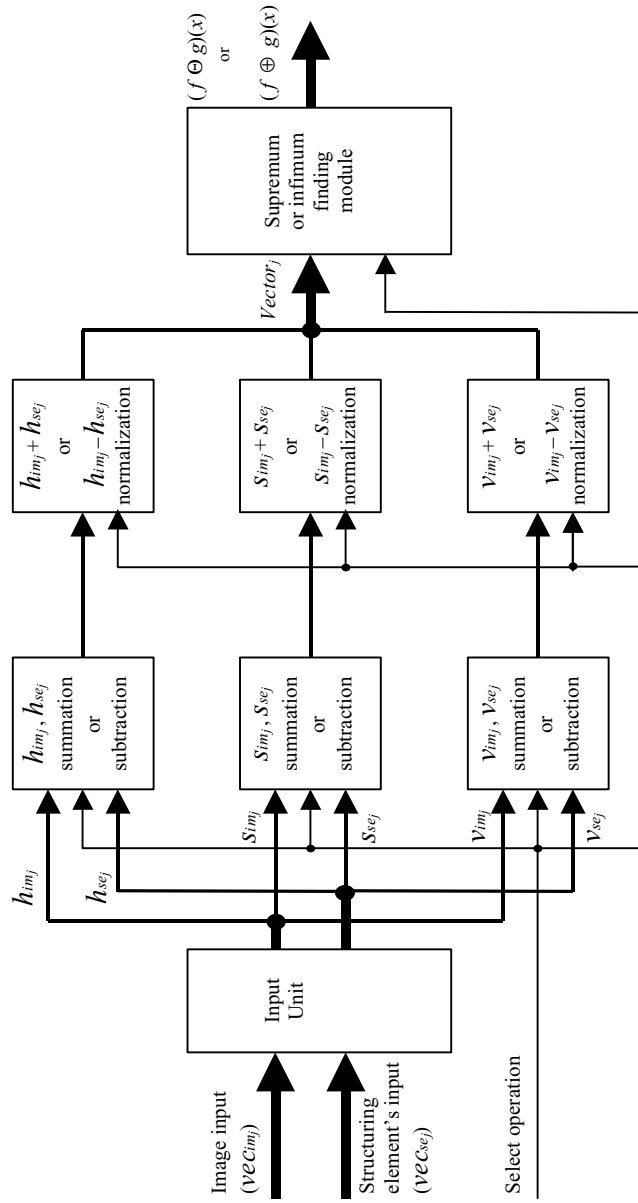


FIGURE 16. Block diagram of a hardware structure that performs vector erosion or dilation of a color input image/by a 3×3 -pixel color structuring element g .

EPF10K30EQC208-1 device of the FLEX10KE Altera device family. The typical system clock frequency is 40 MHz.

VII. CONCLUSIONS

Soft morphological filters are a relatively new subclass of nonlinear filters. They were introduced to improve the behavior of standard morphological filters in noisy environments. In this paper the recent descriptions of soft morphological image processing have been presented. Vector soft mathematical morphology extends the concepts of gray-scale soft morphology to color image processing. The definitions of vector soft morphological operations and their properties have been provided. The use of vector soft morphological filters in color impulse noise attenuation has been also demonstrated. Fuzzy soft mathematical morphology applies the concepts of soft morphology to fuzzy sets. The definitions and the algebraic properties have been illustrated through examples and experimental results. Techniques for soft morphological structuring element decomposition and its hardware implementation have been also described.

Soft morphological operations are based on weighted order statistics. Algorithms for implementation of soft morphological operations include the well-known mergesort and quicksort algorithms for weighted order statistics computation. An approach based on local histogram and a successive approximations technique has been also described. This algorithm is a great improvement in speed for a 5×5 image data window or larger. Soft morphological filters can be implemented in hardware using the threshold decomposition and the majority gate techniques. The threshold decomposition technique is fast, but its hardware complexity is exponentially related both to the structuring element size and the resolution of the pixels. In the majority gate algorithm the hardware complexity is linearly related both to the structuring element size and the resolution of the pixels. A hardware structure that performs vector morphological operations has been also described.

REFERENCES

- Barnett, V. (1976). *J. R. Statist. Soc. A* **139**, 318–355.
Bloch, I., and Maitre, H. (1995). *Pattern Recognition* **28**, 1341–1387.
Comer, M. L., and Delp, E. J. (1998). *The Colour Image Processing Handbook*, Sangwine and Horne, eds., pp. 210–224. London, Chapman & Hall.
David, H. A. (1981). *Order Statistics*, New York, Wiley.
Dougherty, E. R., and Astola, J. (1994). *Introduction to Nonlinear Image Processing*, Bellingham, Wash., SPIE.

- Gasteratos, A., and Andreadis, I. (1999). *IEEE Signal Proc. Letters* **6**, 84–86.
- Gasteratos, A., Andreadis, I., and Tsalides, Ph. (1997a). *Pattern Recognition* **30**, 1571–1576.
- Gasteratos, A., Andreadis, I., and Tsalides, Ph. (1998a). *IEE Proceedings—Vision Image and Signal Processing* **145**, 40–49.
- Gasteratos, A., Andreadis, I., and Tsalides, Ph. (1998b). *IEE Proceedings—Circuits Devices and Systems* **145**, 201–206.
- Gasteratos, A., Andreadis, I., and Tsalides, Ph. (1998c). In *Mathematical Morphology and its Applications to Image and Signal Processing*, H. J. A. M. Heijmans and J. B. T. M. Roerdink, eds., pp. 407–414. Dordrecht, The Netherlands, Kluwer Academic Publishers.
- Giardina, C. R., and Dougherty, E. R. (1988). *Morphological Methods in Image and Signal Processing*, Upper Saddle River, N. J. Prentice Hall.
- Goetcharian, V. (1980). *Pattern Recognition* **12**, 7–15.
- Goutsias, J., Heijmans, H. J. A. M., and Sivakumar, K. (1995). *Computer Vision and Image Understanding* **62**, 326–346.
- Haralick, R. M., Sternberg, R., and Zhuang, X. (1986). *IEEE Trans. Pattern Analysis and Machine Intelligence* **PAMI-9**, 532–550.
- Harvey, N. R. (1998). http://www.spd.eee.strath.ac.uk/~harve/bbc_epsrc.html.
- Koskinen, L., Astola, J., and Neuvo, Y. (1991). *Proc. SPIE Symp. Image Algebra and Morphological Image Proc.* **1568**, 262–270.
- Koskinen, L., and Astola, J. (1994). *J. Electronic Imag.* **3**, 60–70.
- Kuosmanen, P., and Astola, J. (1995). *J. Mathematical Imag. Vision* **5**, 231–262.
- Lee, C. L., and Jen, C. W. (1992). *IEE Proc.-G* **139**, 63–71.
- Matheron, G. (1975). *Random Sets and Integral Geometry*, New York, Wiley.
- Pitas, I., and Venetsanopoulos, A. N. (1990). *Proceedings of the IEEE* **80**, 1893–1921.
- Plataniotis, K. N., Androustos, D., and Venetsanopoulos, A. N. (1999). *Proceedings of the IEEE* **87**, 1601–1622.
- Pu, C. C., and Shih, F. Y. (1995). *Graphical Models and Image Processing* **57**, 522–526.
- Serra, J. (1982). *Image Analysis and Mathematical Morphology: Vol. I*. London, Academic Press.
- Shih, F. Y., and Pu, C. C. (1995). *IEEE Trans. Signal Proc.* **43**, 539–544.
- Shinha, D., and Dougherty, E. R. (1992). *J. Visual Commun. Imag. Repres.* **3**, 286–302.
- Talbot, H., Evans, C., and Jones, R. (1998). In *Mathematical Morphology and Its Applications to Image and Signal Processing*, H. J. A. M. Heijmans and J. B. T. M. Roerdink, eds., pp. 27–34. Dordrecht, The Netherlands, Kluwer Academic Publishers.
- Tang, K., Astola, J., and Neuvo, Y. (1992). In *Proceedings of 6th European Signal Processing Conference*, pp. 1481–1484. Brussels, Belgium.
- Wendt, P. D., Coyle, E. J., and Gallagher, N. C., Jr. (1985). *IEEE Trans. Acoustics Speech and Signal Proc.* **ASSP-34**, 898–911.

